Elsevier Editorial System(tm) for Journal of Quantitative Spectroscopy and Radiative Transfer

Manuscript Draft

Manuscript Number:

Title: Multispectrum analysis of 12CH4 in the v4 band: I. Air-broadened half widths, pressure-induced shifts, temperature dependences and line mixing

Article Type: Special Issue - HITRAN 10

Keywords: Methane; air broadening; pressure-induced shifts; temperature dependence; off-diagonal relaxation matrix elements; line mixing; FTIR spectroscopy

Corresponding Author: Dr. MaryAnn H. Smith,

Corresponding Author's Institution: NASA Langley Research Center

First Author: MaryAnn H. Smith

Order of Authors: MaryAnn H. Smith; D. Chris Benner; Adriana Predoi-Cross; V. Malathy Devi

Multispectrum analysis of $^{12}CH_4$ in the ν_4 band: I. Air-broadened half widths, pressure-induced shifts, temperature dependences and line mixing

M.A.H. Smith[a], D. Chris Benner[b], A. Predoi-Cross[c], V. Malathy Devi[b]

[a] Science Directorate, NASA Langley Research Center, Hampton, VA 23681-2199, USA,
[b] The College of William and Mary, Box 8795, Williamsburg, Virginia 23187-8795, USA,
[c] Department of Physics, University of Lethbridge, 4401 University Drive, Lethbridge, AB, T1K 3M4, Canada.

Number of pages: 23
Number of Figures: 7
Number of Tables: 4 (including Appendix)

Send correspondence to:

Dr. Mary Ann H. Smith
NASA Langley Research Center
Mail Stop 401A
Hampton, VA 23681-2199
Phone: 757-864-2701
Fax: 757-864-7790
E-mail: Mary.Ann.H.Smith@nasa.gov

Keywords: Methane, air broadening, pressure-induced shifts, temperature dependence, off-diagonal relaxation matrix elements, line mixing, FTIR spectroscopy

ABSTRACT

Lorentz air-broadened half widths, pressure-induced shifts and their temperature dependences have been measured for over 430 transitions (allowed and forbidden) in the ν_4 band of $^{12}CH_4$ over the temperature range 210 to 314 K. A multispectrum non linear least squares fitting technique was used to simultaneously fit a large number of high-resolution (0.006 to 0.01 cm^{-1}) absorption spectra of pure methane and mixtures of methane diluted with dry air. Line mixing was detected for pairs of A-, E-, and F-species transitions in the P- and R-branch manifolds and quantified using the off-diagonal relaxation matrix elements formalism. The measured parameters are compared to air- and N_2-broadened values reported in the literature for the ν_4 and other bands. The dependence of the various spectral line parameters upon the tetrahedral symmetry species and rotational quantum numbers of the transitions is discussed. All data used in the present work were recorded using the McMath-Pierce Fourier transform spectrometer located at the National Solar Observatory on Kitt Peak.

1. INTRODUCTION

Accurate measurements of methane air-broadened half width and air-induced pressure shift coefficients, and their temperature dependences, are crucial for accurate remote sensing of terrestrial and other planetary atmospheres. For many years investigators have performed measurements to characterize these parameters, but due to the complex nature of the methane spectrum it is quite challenging to obtain accurate measurements for all transitions. In particular, the pressure-induced shifts in the fundamental bands are difficult to measure since the magnitudes of the shifts are relatively small compared to those in the overtone and combination bands. Determining the temperature dependence of both the widths and pressure-induced shifts from laboratory spectra adds more complexity and difficulty to the analysis process. Sophisticated, modern experimental measurement and analysis techniques have been developed in the past several years to overcome these challenges.

For over two decades our group has used the McMath-Pierce Fourier transform spectrometer (FTS) located on Kitt Peak, Arizona, to record high-resolution spectra of a number of molecular species, including CH_4 and its isotopologues. From a previous analysis of some of these FTS spectra, Smith et al.[1] have reported measurements of air- and N_2-broadened half widths, pressure-induced shifts and their temperature dependences for approximately 150 transitions in the ν_4 band. The positions and relative intensities of those transitions were also determined. Numerous other studies of pressure broadening and pressure-induced shift coefficients in the vibration-rotation bands of methane broadened by air, N_2, and O_2 are available in the literature [2-44]. A number of studies of CH_4 line mixing have been reported [15,17,37,39-42,45-48], but only two [17,47] include the ν_4 band.

The present study was initiated to extend the measurements reported in Ref. [1] to higher J values in the ν_4 band and to retrieve more accurate values of the broadening and shift coefficients and their temperature dependences by using a modified multispectrum fitting algorithm. In the previous study [1] each spectrum was fitted separately, and the final results for the various spectral line parameters were obtained by fitting the individually retrieved values to the expected relationships of half width or shift vs. pressure and temperature. In the present work we simultaneously fitted a large number of spectra obtained at different physical conditions (sample pressures, absorption path lengths, gas temperatures) using a multispectrum technique [49] to directly obtain a set of spectroscopic parameters consistent with all the spectra. In addition, we

also measured the line mixing coefficients (via the off-diagonal relaxation matrix formalism) between pairs of transitions involving a specific set of propensity rules as described by Pieroni et al. [46]. Pine and Gabard [42] have also used multispectrum fits in their study of line mixing in the Q branch of the ν_3 band of methane. However, the investigators in Ref. [42] used a different line mixing approximation to quantify the line mixing effects.

In this paper results from the analysis of the ν_4 band of methane broadened with air at various sample temperatures in the 210 to 314 K range are presented. A large number of spectra were fit simultaneously to retrieve precise experimental values of several line parameters including positions, intensities, broadening and shift coefficients, temperature dependences of half width and, pressure-shift coefficients. Methane and air were used as broadening gases and the self- and air-broadened spectra were analyzed simultaneously. Because of the large amount of line parameters retrieved, the results corresponding to self-broadening are reported in a separate article [50].

2. EXPERIMENTAL DETAILS

The McMath-Pierce Fourier transform spectrometer (FTS) at the National Solar Observatory (NSO) on Kitt Peak was used to record the spectra. Unapodized resolutions of 0.006 cm^{-1} and 0.01 cm^{-1} were used to record the low pressure methane spectra and pressure-broadened spectra, respectively. The experimental set up included a glower source, liquid helium cooled As-doped silicon detectors and a KCl beam splitter. In the initial experiments performed several years ago [1], premixed samples of dilute high-purity natural CH_4 in dry-air were used to collect the air-broadened data. In the more recent experiments, commercially purchased dry-air samples were mixed with high purity natural samples of CH_4 to obtain the desired volume mixing ratios of methane in air. Similar to the previous study [1], the sample pressures and temperatures were monitored continually for each spectrum during the entire recording period (approximately an hour to 90 minutes depending upon the number of interferograms co-added for each spectrum). For most of the spectra the signal-to-noise ratios were ~1000. The experimental conditions of the 60 spectra analyzed are listed in Table 1. Self-broadened CH_4 spectra are included in this table because they were simultaneously analyzed with the air-broadened spectra.

The absorption path lengths of the air-broadened spectra were between 5 cm and 150 cm, and all cold spectra were obtained using the 50 cm coolable cell described in Ref. [1]. A brief

description of the coolable cell is given here: the cell was designed and built at the NASA Langley Research Center and consists of a double-walled Pyrex glass tube with an internal diameter of 7.6 cm with approximately 0.5 cm spacing between the walls. KCl windows were attached to the ends of the cell and the entire cell assembly was mounted inside a cylindrical aluminum chamber that was evacuated to prevent condensation when the inner cell is cooled. T-type thermocouples were attached at 8 different locations on the outside wall of the gas cell to monitor the sample temperatures. Chilled denatured ethanol is circulated through the space between the double walls of the cell to cool the gas mixtures.

A compressed plot of an air-broadened methane spectrum in the 1100 to 1600-cm^{-1} region is presented in Fig. 1. The methane-air mixture had a methane volume mixing ratio of ~0.16, a total pressure of ~256 torr, and a temperature of 294.2 K. The gas mixture was contained in a 50-cm absorption cell. Transitions belonging to both the ν_4 and ν_2 bands of $^{12}CH_4$ are apparent in the spectrum as well as numerous water vapor lines, mostly belonging to the ν_2 band.

Table 1 includes the spectra that were used in our previous investigation of the ν_4 band [1]. Additional data recorded in recent years include self-broadened spectra recorded over a wide range of pressures and temperatures as well as air-broadened spectra with higher volume mixing ratios of methane to extend the previous measurements [1] to higher J values in both the P and R branches. Measurements for only P- and R-branch manifolds are reported here. Because of the congested and complex structure of the Q branch, the analysis is more difficult, and results for the Q branch will be reported in a later paper.

3. DATA RETRIEVALS AND ANALYSIS

The first step in the multispectrum analysis is to calibrate the wavenumber scales for all the spectra included in the fit, using the same reference standard. This procedure is important in order to retrieve precise line center positions and pressure-induced shifts. The spectra analyzed in this study were recorded during several experiments that took place over a period of nearly two decades, but all contained residual water vapor lines. Therefore we have used the positions of the ν_2 band water vapor lines to calibrate the wavenumber scales of all the spectra. Each of these water lines had a narrow component superimposed on a broad component. The narrow water vapor lines were due to the residual air (~0.01 to 0.03 torr) present inside the vacuum tank enclosing the FTS, and the broad water vapor features arose from the nitrogen purged optical

paths (at ambient pressure ~600 torr) between the source and the cell and also between the cell and the entrance aperture of the FTS. The position of the narrow component of each water vapor feature was used in calibrating the spectra. The depths of water vapor lines used in the calibration process varied from spectrum to spectrum because of the day-to-day differences in the residual water amounts in the FTS tank and in the nitrogen-purged optical paths.

The multispectrum fitting technique allows us to simultaneously fit a number of spectra over a specified wavenumber interval. In some cases (mostly for linear molecules) an entire band can be fit using a broad wavenumber interval and all of the recorded spectra [51,52]. Because of the complex nature of the methane spectra (Q branch, P and R manifolds, and the varying amounts of water vapor from one spectrum to another) only short spectral segments 5 to 15 cm^{-1} wide could be fit at a time using subsets of the entire group of spectra. The number of spectra included in each fit depended upon the depths of the methane absorption features. In the spectral regions containing high-J CH_4 transitions where the absorption is weak, the spectra recorded with short path lengths were not used.

In the multispectrum fitting technique it was possible to retrieve simultaneously values for all the line parameters including values for the temperature dependences of half width and pressure-induced shift coefficients for both self- and air-broadening. Details of the analysis procedure are given in several of our previous studies [14,51,52]. In the fitting algorithm the experimental spectra and the synthetic spectra are matched by minimizing the sum of the squares of the residuals between the two. This was achieved by adjusting the values of the various line parameters mentioned above. Eqs. (1-3) were used to determine the half widths and pressure shift coefficients,

$$b_L(p,T) = p \times \left[b_L^0(air)(p_0,T_0) \times (1-\chi) \times \left[\frac{T_0}{T}\right]^{n1} + b_L^0(self)(p_0,T_0) x \chi \left[\frac{T_0}{T}\right]^{n2} \right] \quad (1)$$

$$\nu = \nu_0 + p\left[\delta^0(air)(1-\chi) + \delta^0(self)\chi\right] \quad (2)$$

$$\delta^0(T) = \delta^0(T_0) + \delta'(T - T_0) \quad (3)$$

In the above equations, $b_L{}^0$ and δ^0 represent pressure-broadened half width and pressure-induced shift coefficients, respectively (in $cm^{-1}atm^{-1}$ at 296 K) at the reference pressure p_0 (1 atm) and temperature T_0 (296 K) of the broadening gas (either air or methane). b_L (p, T) is the

Lorentz half width (in cm^{-1}) of the spectral line at pressure p and temperature T, and χ is the ratio of the partial pressure of methane to the total sample pressure in the cell. The temperature dependence exponents of air- and self- broadened half width coefficients are given by n_1 and n_2, respectively and δ' corresponds to the temperature dependence coefficient of the pressure-induced line shift.

The initial line list used in the analysis consisted of line positions, intensities, air- and self-broadened half width, air- and self-induced pressure-shift coefficients and the temperature dependence exponents for air-broadened half width coefficients. These values were taken from the HITRAN04 line parameters compilation [53]. In our initial line list the temperature dependence exponents for air- and self-broadened half widths, n_1 and n_2, were assumed to be the same (i.e., n_1) for a given transition. The n_1 values given in the HITRAN04 database [53] range approximately between 0.63 and 0.80. The temperature dependence coefficients δ' of self- and air-induced pressure shifts were set to a default initial value of zero for all transitions. Line parameters for unmeasured transitions were held fixed to the values given in the HITRAN04 database [53] or the initial default values as described above.

While fitting certain spectral regions it became clear that we were not able to fit all the spectra to their noise levels, especially the spectra with higher sample pressures. The residuals between the experimental and calculated spectra indicated that there must be mixing occurring between certain pairs of transitions. These residuals could significantly be reduced by taking into account the line mixing effects in the least squares solutions and accordingly, the off diagonal relaxation matrix elements coefficients were introduced into the multispectrum fittings following the method developed by Levy et al. [54]. The fitting of the mixed pairs was guided by the observed residuals and by the propensity rules for methane as outlined by Pieroni et al. [46]. Figure 2 shows an example of the residuals for spectra fitted without and with line mixing in the R(11) manifold of $^{12}CH_4$.

Effects due to Dicke narrowing were not observed in our data because the resolution in the pressure-broadened spectra was ~0.01 cm^{-1} while the Doppler half widths of the transitions were ~0.0021 cm^{-1}. Neither the resolution nor the signal-to-noise ratios in our spectra were sufficient to determine the speed dependence parameters for the transitions observed.

4. RESULTS AND DISCUSSION

The Appendix lists the measured air-broadened half width and air-induced shift coefficients, the temperature dependence exponents of air-broadened half width coefficients, and the temperature dependence of air-shift coefficients. The results in the Appendix are sorted in terms of $|m|$ where m equals $-J$ for P transitions, J for Q transitions, and $J+1$ for R transitions. The first column lists $|m|$, the second column denotes the type of transition (R, Q or P), and the third column lists the vibrational code (v_b=3) used to identify the band. The next few columns list the upper and lower state quantum numbers J, C ($A1$, $A2$, $F1$, $F2$, E), and n (the prime denotes the upper state and the double prime denotes the lower state). The last five columns give the measured line position in cm^{-1}, and the air-broadened half width, the temperature-dependence exponent of the half width, the air pressure-induced shift, and the temperature-dependence coefficient of the shift. The statistical uncertainties given in parentheses correspond to one standard deviation of uncertainty in the measured quantities in units of the last quoted digit. Mean values and standard deviations of the measured parameters for each $|m|$ and C″ of the allowed transitions are listed in Table 2 for $|m|$ up to 9. The results for self-broadening are reported elsewhere [50].

An inspection of the values listed in the Appendix shows the high precision achieved in the retrieved air-broadened half width and shift parameters. By fitting a large number of spectra simultaneously the random errors such as those due to the noise levels of the spectra are minimized. In order to account for the absolute uncertainties in the retrieved parameters, errors in the measurements of experimental conditions must be accounted for. These errors include uncertainties in the measurements of gas pressures and temperatures, in the wavenumber calibration of the spectra, errors in the spectral line shapes used in the fits, and uncertainties in line parameters such as position, intensity, and widths which were fixed in the solution (for weak absorptions and for transitions whose parameters could not be retrieved due to severe overlap or blend). The determination of the magnitudes of all these errors is not trivial. The absolute one sigma standard deviations in our measured parameters are estimated to be 1% in half width coefficients, 10-15% in pressure-induced shift coefficients, 10% in n and 20-50% in the temperature dependence coefficients of the pressure-induced shifts (δ′), added to the errors listed

in the Appendix. The estimated errors for δ′ are high because the range in the temperatures of the spectra is not large enough to retrieve accurate values for these parameters.

We have obtained measurements for over 430 transitions (including the allowed and forbidden transitions) in the ν_4 band of $^{12}CH_4$, but it was not possible to determine all line parameters for each listed transition, particularly for the weakest lines and those that are overlapped by the numerous Q branch lines. The goal was to measure accurate parameters for as many lines as possible so that these results could be used to develop a reliable theoretical model. We may recall that the total number of transitions listed for the dyad region of methane in the HITRAN 2004 database [53,55] is 65,478. The difference between this total and the small number for which broadening and shift parameters have been measured illustrates the need to develop a reliable theoretical model to predict these parameters for unmeasured transitions.

4.1 Air-broadened half widths and temperature dependences

Figs. 3(a) and 3(b) illustrate the variation of b_L^0 (air) and its temperature dependence exponent n as a function of m. In the figures the half width coefficients and temperature exponents are plotted using different symbols for A-, E- and F-species transitions. We observe in the present work, as has been noted in several previous methane studies, that for a given m, the smallest half width coefficients generally belong to E-species transitions. It is obvious that for each value of m there is a large range of measured air-broadened half width coefficient values; while we have examined the variation of the half widths with the upper and lower secondary quantum indices n' and n'' for a given $|m|$ and symmetry, no clear dependence on n' or n'' could be determined from our data. We also note that the larger half width coefficients appear to be associated with forbidden transitions. The largest measured air-broadened half width coefficient in the present work is ~0.08 $cm^{-1}atm^{-1}$ at 296 K corresponding to ~$|m|$=5 and the smallest values of <0.02 $cm^{-1}atm^{-1}$ at 296 K are obtained for $|m|$=16−20.

In Figs. 4(a) and 4(b) the air-broadened half width coefficients and temperature exponents from the present work are compared to those measured in the previous study [1]. As in Fig. 3, the parameters are plotted as a function of m, but here the A-, E- and F-species transitions are not distinguished by different symbols. From Fig. 4 it is clear that the air-broadening and shift parameters were determined to much higher values of J in the present work than in Ref. [1]. The ratio of the Ref. [1] value to the present-work value for the same transition is plotted in Figs.

4(c) and 4(d). The differences between the present and previous [1] air-broadened half width coefficients are less than ±2%, with a few exceptions. For the temperature exponents of the air-broadened half widths, the values obtained in the previous study [1] are, on average, 12% smaller than those obtained for the same transitions in the present work, and the differences are increasing with $|m|$. These differences between Ref. [1] and the present work that we see in Figs. 4(c) and 4(d) are most likely related to the differences in analysis techniques and line shape models used in the two studies, already mentioned in Section 1 of this paper.

Figs. 3(b) and 4(b) indicate that most values of n lie within the range of 0.75 to 1.05 throughout the range of $|m|$ measured. In Fig. 4(d) the ratios of n values from Ref. [1] to the present work show a large scatter. The retrieved values of n from the present work are, on average, 12% larger than those measured in Ref. [1], and the differences are larger for weaker transitions at higher $|m|$. The number of air-broadened spectra used in this study is more than twice that in Ref. [1], but the increased number of spectra should not produce such large differences in n. The CH_4 volume mixing ratios in many of the air-broadened spectra used in this work are significantly higher than in Ref. [1], allowing absorption features that were fairly weak in the previous study to be measured more precisely in this work. This fact, combined with the inherent advantage of simultaneously fitting multiple spectra, results in more accurate determinations of the air-broadened half width coefficients and their temperature dependences in the present work.

We have compared our air-broadened widths with other published air-broadening measurements in the ν_4 band, mainly the TDL studies of Malathy Devi et al. [12] and Varanasi and Chudamani [20,21], and found no differences larger than the uncertainties of the measurements. There are no published direct measurements of n values for air-broadened widths in the ν_4 band other than Ref. [1]. However, our n values for air-broadened widths are consistent with the N_2-broadening n values from TDL measurements in the ν_4 band [7,20,21,43].

We have also compared our mean air-broadened half width coefficients in the ν_4 band (Table 2) to the mean air-broadened half width coefficients for transitions with the same lower state C'' and n'' in the $\nu_2+\nu_3$ band [14]. The mean values for each |m| are quite close (within ±1% or better) for $|m|$ values up to 11. Beyond $|m| = 10$ or 11, there are fewer transitions in the two bands to compare and the values scatter slightly more than for lower values $|m|$. It should be noted that the upper state C′ and n′ and the vibrational code are different for the two bands.

Finally, referring back to Fig. 3(a) and (b) where the measured values of b_L^0(air) and n (air) are plotted vs. m, as well as Table 2, we note that our results show a small positive correlation, such that larger n (air) values are associated with larger b_L^0(air) values. A similar observation was made in an earlier study of air-broadening in the methane bands in the 2.3-μm region [10].

4.2 Air-induced shift coefficients and their temperature dependences

The measured values of δ^0(air) and δ'(air) are plotted in Figs. 3(c) and 3(d) as functions of m, and they are compared with the results of Ref [1] in Fig. 5. The majority of the measured air-shift coefficients listed in the Appendix show large scatter for each m value, and, as for the broadening coefficients, there is no obvious variation of the shift values with the quantum numbers C'' and n''. Most measured air shift coefficients range between −0.002 and −0.005 $cm^{-1}atm^{-1}$ at 296K; the mean and standard deviation of all measured air shift coefficients is -0.0033 ± 0.0022 $cm^{-1}atm^{-1}$ at 296K. We estimate that the error that could be introduced in the air-shift coefficients for the measured transitions by fixing the values of unmeasured transitions to 0.002 $cm^{-1}atm^{-1}$ at 296 K is insignificant. The plots in Figs. 3(c) and 3(d) and the mean values in Table 2 indicate that δ^0(air) becomes somewhat more negative as $|m|$ increases, but there is no discernable dependence of δ'(air) on $|m|$. We note that more negative air-induced shifts as |m| increases have also been observed in the octad region [14], particularly for the $\nu_1+\nu_4$ band.

As we have done in Fig. 4 for air-broadened half width coefficients and their temperature dependences, in Fig. 5 we compare the previous [1] and present measurements of the air-induced shift coefficients and their temperature dependences in the ν_4 band**.** However, because of the small magnitudes and relatively large error bars of the δ^0 and δ' values, in Figs. 5(c) and (d), we show the differences between the previous [1] and present measurements rather than the ratios. The majority of the measured values of δ' in the present work range between -0.25×10^{-5} and $+0.5\times10^{-5}$ $cm^{-1}atm^{-1}K^{-1}$ whereas in Ref. [1] the range of δ' was $\sim \pm0.25\times10^{-5}$ $cm^{-1}atm^{-1}K^{-1}$. This level of agreement in δ' between the two studies is encouraging considering the small magnitude of this parameter and the two different analysis techniques used to determine the values.

4.3 Off-Diagonal Relaxation Matrix Element Coefficients

Collisional effects result in the transfer of intensity from some parts of the spectrum to others which consequently results in an interference effect between lines sometimes referred to

as "*collisional line mixing*" [54]. This effect may be quantified using the relaxation matrix and the off-diagonal matrix elements to accurately represent the coupling between transition pairs. The spectral line profiles in the multispectrum fittings accounted for these effects using an asymmetric component (proportional to pressure) via the speed-dependent Voigt profile. Because the range in temperatures of the gas samples was limited in the present study, the temperature dependence exponents of the off-diagonal relaxation matrix element coefficients were fixed to the value 1.0 (see Ref. [15]) and were not uniquely solved for.

In mathematical formulation, the spectral profile I(ω) may be written according to matrix form for any number of pressure induced profiles, N, as a function of the wavenumber ω:

$$I(\omega) = \mathbf{X}^T \left(\boldsymbol{\omega} - \boldsymbol{\omega}_\mathbf{0} - i\mathbf{W}\right)^{-1} \boldsymbol{\rho}\mathbf{X}. \tag{4}$$

In Eq. (4) W represents the relaxation matrix and *i* is the imaginary number (defined as the square root of negative one). The diagonal elements of W are the sum of the Lorentz half width s and pressure-induced shift coefficient of a given transition. The symbol ω_0 represents an N × N diagonal matrix whose diagonal elements correspond to zero pressure line positions and ω is a similar N × N diagonal matrix in which the diagonal elements ω_{jj} of the matrix represents the wavenumber. ρ is a diagonal N × N density matrix and X^T is the matrix transpose of the 1 × N matrix X defined as,

$$X_j = \sqrt{\frac{S_j}{\rho_j}}. \tag{5}$$

The ratio of intensity to the number density given by Eq. (5) in the lower state corresponds to the j^{th} spectral line. The off-diagonal matrix elements of W are connected by the detailed balance equation given below in Eq. (6) where k represents the other spectral line involved in the line coupling:

$$W_{jk} = W_{kj} \frac{\rho_j}{\rho_k} \tag{6}$$

Line mixing was detected in 57 pairs of transitions and measured using the off-diagonal relaxation matrix element (ORME) coefficients. We were able to determine the mixing parameters in *J*-manifolds of the P and R branches for $3 \leq |m| \leq 18$; pairs of transitions corresponding to all three symmetry species (A, E, F) were measured. The measured ORME coefficients (in cm^{-1} atm^{-1} at 296 K) determined for air mixing are listed in Table 3.

The ORME coefficients measured in this air-broadening study are plotted vs. *m* in Fig. 7(a), and in Fig. 7(b) they are compared with measured air-broadened ORME coefficients for matching transitions in the $\nu_2+\nu_3$ band [15]. N_2-broadened line mixing parameters from matching transitions in theν_3 band [37,40]. The two ν_3 studies determined the line mixing coefficients using the Rosenkranz approximation [56]. Theν_3 values plotted in Fig. 7(b) are estimated from the Rosenkranz coefficients published in Refs. [37,40] and not strictly comparable with results obtained via the ORME formalism. Nevertheless, considering the absolute uncertainties of the experimentally-determine mixing parameters, the agreement between corresponding pairs of transitions in various bands is quite good, and the N_2-broadened mixing parameters are not substantially different from the air-broadening values.

5. SUMMARY AND CONCLUSIONS

Measurements of air-broadened half width and pressure-induced air shift coefficients and their temperature dependences for over 430 individual transitions in the ν_4 band of $^{12}CH_4$ have been obtained by analyzing up to 60 spectra simultaneously using a multispectrum fitting technique, thus extending the previous measurements [1] from J'=14 to J'=20. The present study has increased the number of measured ν_4 transitions from ~150 [1] to over 430. The measured transitions in the present work also include a number of forbidden transitions. Comparisons of the present measurements of air-broadened width and pressure-induced shift coefficients and their variations with temperature show general agreement with results obtained in the previous study [1] using a spectrum-by-spectrum analysis method. Addition of high-abundance spectra, along with use of the multispectrum fitting technique for analysis, has made it possible not only to extend the previous measurements to much higher values of *J* but also to increase the precision and accuracy in the various measured parameters.

Line mixing coefficients using the off-diagonal relaxation matrix element formalism have also been measured in different pairs of transitions for a number of *J* manifolds of both the P- and R-branches in all three symmetry species. This study reports the first extensive measurements of line mixing at terrestrial atmospheric pressures in the ν_4 fundamental band, using the off-diagonal relaxation matrix element coefficients.

There is good general agreement among the line mixing measurements for air broadening from the present work with air broadening measurements in the $\nu_2+\nu_3$ band [15] and N_2-

broadening results in the ν_3 band [37,40]. Even though the spectra used in this work were recorded at various temperatures between 210 and 314 K, this temperature range was not significant enough to allow us to determine reliable values for temperature dependence exponents of line mixing coefficients. One important point to note here is that it was envisioned [14,57] that the apparently random distribution of the pressure-induced shifts with rotational quantum numbers could be associated with possible line mixing effects neglected in the analysis. But this point could not be fully validated by the present work or by Ref. [15]. Fitting all the data simultaneously and taking into account the line mixing effects in the least squares fits did remove some of the scatter in the distribution of the measured pressure-induced shifts. More theoretical developments and possibly additional experimental studies may be required to unravel this point.

ACKNOWLEDGMENT

The authors thank Claude Plymate and Mike Dulick of the National Solar Observatory for their assistance with the FTS laboratory measurements at Kitt Peak. We also thank Linda Brown of the Jet Propulsion Laboratory for reading the manuscript and providing helpful comments. Research at the College of William and Mary is supported under contracts and cooperative agreements with the National Aeronautics and Space Administration. A. Predoi-Cross acknowledges the support received from the National Sciences and Engineering Research Council of Canada (NSERC). NASA's Upper Atmosphere Research Program provides funding to the National Solar Observatory for support of NASA activities at the McMath-Pierce FTS laboratory facility.

Table captions

1. Summary of experimental conditions of CH_4 spectra
2. Mean air-broadened half width and pressure-induced shift coefficients and their temperature dependences for allowed P and R transitions in the ν_4 band of $^{12}CH_4$.
3. Off-diagonal relaxation matrix element (ORME) coefficients measured for air-broadening in the ν_4 band of $^{12}CH_4$.

Appendix. Supplementary data

Measured spectral line parameters for air-broadening in the methane ν_4 band sorted by $|m|$.

Figure captions

1. An air-broadened methane spectrum in the 1100 to 1600 cm^{-1} spectral range. The spectrum was obtained with a methane volume mixing ratio of ~0.16. The total pressure is ~256 torr in a 50-cm absorption path at 294.2 K. Transitions belonging to both the ν_4 and the ν_2 bands are visible, and the band centers are indicated on the plot. The broad feature near 1260 cm-1 is an artifact of the optics used to record the spectrum. The zero signal level is shown by a horizontal dashed line at the bottom of the plot.

2. Observed spectra (lower panel) and residuals from a multispectrum fit without (upper panel) and with line mixing (middle panel) in the R(11) manifold of the $^{12}CH_4$ ν_4 band. This preliminary fit was performed on 15 room-temperature self- and air-broadened CH_4 spectra recorded with cell lengths of 0.00958, 0.250, and 1.50 m (see Table 1). The maximum total pressures were 550.1 torr for air-broadening and 453.3 torr for self-broadening. The large residuals near 1364.4 cm^{-1} in the upper panel are due to strong mixing between the 12F2 1 ←11F1 3 and 12F1 1 ← 11F2 3 transitions. The smaller residuals between 1365 and 1367 cm^{-1} are due to weaker mixing between the 12F2 2 ← 11F1 2 and 12F1 2 ← 11F2 2 transitions.

3. Measured air-broadened half width coefficients, b_L^0 (a), temperature exponents of the widths (b), pressure-induced shifts (c), and temperature coefficients of the shifts (d) for the ν_4 band of $^{12}CH_4$ broadened by air, all plotted as a function of $\boldsymbol{m}$. Different symbols are used for the A-, E- and F-species transitions. Where error bars are not visible, they are smaller than the size of the symbols used. The plotted values are tabulated in the Appendix.

4. Measured air-broadened half width coefficients (a) and temperature dependence exponents (b) compared with those from the previous study [1], and the ratios of air-broadened half width coefficients (c) and temperature dependence exponents (d) from Ref. [1] divided by values from present work, plotted as functions of $\boldsymbol{m}$. The dashed horizontal lines in (c) and (d) correspond to a ratio of 1.00. Where error bars are not visible, they are smaller than the size of the symbols used in the plot.

5. Measured air pressure-induced shift coefficients (a) and temperature dependences (b) compared with those from the previous study [1], and the differences of air-broadened shift coefficients (c) and temperature dependences (d) from the present work values, plotted as functions of ***m***. The dashed horizontal lines in (c) and (d) correspond to zero difference. Where error bars are not visible, they are smaller than the size of the symbols used in the plot.

6. Measured air-broadened half width coefficients (a), air half width temperature exponents (b), and air pressure-induced shifts (c) from the present work are plotted against the corresponding values listed in the HITRAN04 database [53].

7. Measured off-diagonal relaxation matrix element coefficients (in $cm^{-1}atm^{-1}$ at 296 K), plotted vs. *m*. (a) Air-broadening values obtained in the present work. (b) Present work values compared with measured air- and N_2-broadening values for matching transitions from other bands[15,37,40].

Reference List

[1] Smith MAH, Rinsland CP, Malathy Devi V, Benner DC. Temperature dependence of broadening and shifts of methane lines in the nu4 band. Spectrochimica Acta 1992; 48A:1257-1272.

[2] Antipov AB, Kochanov VP, Sapozhnikova VA, Tinchurina EG. Collisional broadening and shift of the 3.39-MUm line of the nu3 band of methane. Opt Spektrosk 1989; 66:64-68.

[3] Antipov AB, Pyrsikova PD, Sapozhnikova VA. Effect of temperature and pressure on the profile of the methane absorption line with its center at nu0 = 2947.9 cm-1. Opt Spektrosk 1976; 40:795-799.

[4] Benner DC, Malathy Devi V, Smith MAH, Rinsland CP. Air-, N2-, and O2-broadening and shift coefficients in the nu3 spectral region of 12CH4. J Quant Spectrosc Radiat Transfer 1993; 50:65-89.

[5] Clark HY, Corner L, Denzer W, Hancock G, Hutchinson A, Islam M, Peverall R, Ritchie GAD. Difference frequency generation in periodically poled lithium niobate and its use in the detection of atmospheric methane. Chem Phys Lett 2004; 399:102-108.

[6] Kapitanov VA, Ponomarev YuN, Tyryshkin IS, Rostov AP. Two-channel opto-acoustic diode laser spectrometer and fine structure of methane absorption spectra in the 6070 - 6180 cm-1 region. Spectrochim Acta 2007; A 66:811-818.

[7] Lepere M, Valentin A, Henry A, Camy-Peyret C, Blanquet G, Populaire J-C, Mantz AW. Pressure broadening study at low temperature: application to methane. Spectrochim Acta 2002; A 58:2413-2419.

[8] Lepere M, Valentin A, Henry A, Camy-Peyret C, Lengele M, Populaire J-C, Blanquet G. Diode laser spectroscopy: Temperature dependence of R(0) line in the nu4 band of CH4 perturbed by N2 and O2. J Mol Spectrosc 2005; 233:86-92.

[9] Malathy Devi V, Benner DC, Smith MAH, Rinsland CP. Measurements of air-broadening and pressure-shifting of methane lines in the 2.3 mum region. J Mol Spectrosc 1993; 157:95-111.

[10] Malathy Devi V, Benner DC, Smith MAH, Rinsland CP. Temperature dependence of Lorentz air-broadening and pressure-shift coefficients of 12CH4 lines in the 2.3-mum spectral region. J Quant Spectrosc Radiat Transfer 1994; 51:439-465.

[11] Malathy Devi V, Fridovich B, Snyder DGS, Jones GD, Das PP. Tunable diode laser measurements of intensities and Lorentz broadening coefficients of lines in the nu2 band of 12CH4. J Quant Spectrosc Radiat Transfer 1983; 29:45-47.

[12] Malathy Devi V, Rinsland CP, Smith MAH, Benner DC. Measurements of 12CH4 nu4 band halfwidths using a tunable diode laser system and a Fourier transform spectrometer. Appl Opt 1985; 24:2788-2791.

[13] Pine AS. High-resolution methane nu3-band spectra using a stablized tunable difference-frequency laser system. J Opt Soc Am 1976; 66:97-108.

[14] Predoi-Cross A, Brawley-Tremblay M, Brown LR, Malathy Devi V, Benner DC. Multispectrum analysis of 12CH4 from 4100 to 4635 cm-1: II. Air-broadening coefficients (widths and shifts). J Mol Spectrosc 2006; 236:201-215.

[15] Predoi-Cross A, Unni AV, Heung H, Malathy Devi V, Benner DC, Brown LR. Line mixing effects in the nu2+nu3 band of methane. J Mol Spectrosc 2007; 246:65-76.

[16] Rinsland CP, Malathy Devi V, Smith MAH, Benner DC. Measurements of air-broadened and nitrogen-broadened Lorentz width coefficients and pressure shift coefficients in the nu4 and nu2 bands of 12CH4. Appl Opt 1988; 27:631-651.

[17] Tran H, Flaud P-M, Gabard T, Hase F, von Clarmann T, Camy-Peyret C, Payan S, Hartmann J-M. Model, software, and database for line-mixing effects in the nu3 and nu4 bands of CH4 and tests using laboratory and planetary measurements. I. N2 (and air) broadenings and the Earth atmosphere. J Quant Spectrosc Radiat Transfer 2006; 101:284-301.

[18] Varanasi P. Air-broadened line widths of methane at atmospheric temperatures. J Quant Spectrosc Radiat Transfer 1975; 15:281.

[19] Varanasi P, Chudamani S. Measurement of pressure-induced shifts of infrared lines with a tunable diode laser. J Quant Spectrosc Radiat Transfer 1989; 41:173-176.

[20] Varanasi P, Chudamani S. Measurements of collision-broadened line widths in the 7.66-mum band of 12CH4 at temperatures relevant to the atmosphere. J Geophys Res 1989; 94:13073-13078.

[21] Varanasi P, Chudamani S. The temperature dependence of lineshifts, linewidths and line intensities of methane at low temperatures. J Quant Spectrosc Radiat Transfer 1990; 43:1-11.

[22] Zeninari V, Parvitte B, Courtois D, Kapitanov VA, Ponomarev YuN. Measurements of air and noble-gas broadening and shift coefficients of the methane R3 triplet of the 2nu3 band. Appl Phys B 2001; 72:953-959.

[23] Darnton L, Margolis JS. The temperature dependence of the half widths of some self- and foreign-gas-broadened lines of methane. J Quant Spectrosc Radiat Transfer 1973; 13:969-976.

[24] Dufour G, Hurtmans D, Henry A, Valentin A, Lepere M. Line profile study from diode laser spectroscopy in the 12CH4 2nu3 band perturbed by N2, O2, Ar, and He. J Mol Spectrosc 2003; 221:80-92.

[25] Fox K, Jennings DE. Measurements of nitrogen-, hydrogen-, and helium-broadened widths of methane lines at 9030-9120 cm-1. J Quant Spectrosc Radiat Transfer 1985; 33:275-280.

[26] Fox K, Jennings DE, Stern EA, Hubbard R. Measurements of argon-, helium-, hydrogen-, and nitrogen-broadened widths of methane lines near 9000 cm-1. J Quant Spectrosc Radiat Transfer 1988; 39:473-476.

[27] Fox K. Symmetry-dependent broadening parameters for methane. J Chem Phys 1984; 80:1367-1368.

[28] Fox K, Quillen DT, Jennings DE, Wagner J, Plymate C. Methane spectral line widths and shifts, and dependencies on physical parameters. J Geophys Res 1991; 96:17483-17488.

[29] Fox K, Jennings DE. Spectroscopic studies of methane in collisions with rare gas atoms and diatomic molecules. J Mol Struct 1990; 224:1-6.

[30] Frankenberg C, Warneke T, Butz A, Aben I, Hase F, Spietz P, Brown LR. Pressure broadening in the 2nu3 band of methane and its implication on atmospheric retrievals. Atmos Chem Phys 2008; in press.

[31] Gerritsen HJ, Heller ME. High-resolution tuned-laser spectroscope. Appl Opt Suppl 1965; 2:73-77.

[32] Gharavi M, Buckley SG. Diode laser absorption spectroscopy measurement of linestrengths and pressure broadening coefficients of the methane 2nu3 band at elevated temperatures. J Mol Spectrosc 2005; 229:78-88.

[33] Keffer CE, Conner CP, Smith WH. Pressure broadening of methane lines in the 6190 A and 6825 A bands at room and low temperatures. J Quant Spectrosc Radiat Transfer 1986; 35:495-499.

[34] Malathy Devi V, Fridovich B, Jones GD, Snyder DGS. Strengths and Lorentz broadening coefficients for spectral lines in the nu3 and nu2 + nu4 bands of 12CH4 and 13CH4. J Mol Spectrosc 1983; 97:333-342.

[35] Menard-Bourcin F, Menard J, Boursier C. Temperature dependence of rotational relaxation of methane in the 2nu3 vibrational state by self- and nitrogen-collisions and comparison with line broadening measurements. J Mol Spectrosc 2007; 242:55-63.

[36] Mondelain D, Chelin P, Valentin A, Hurtmans D, Camy-Peyret C. Line profile study by diode laser spectroscopy in the 12CH4 nu2+nu4 band. J Mol Spectrosc 2005; 232:40-48.

[37] Mondelain D, Payan S, Deng W, Camy-Peyret C, Hurtmans D, Mantz AW. Measurement of the temperature dependence of line mixing and pressure broadening parameters between 296 and 90 K in the nu3 band of 12CH4 and their influence on atmospheric methane retrievals. J Mol Spectrosc 2007; 244:130-137.

[38] Neshyba SP, Lynch R, Gamache RR, Gabard T, Champion JP. Pressure-induced widths and shifts for the nu3 band of methane. J Chem Phys 1994; 101:9412-9421.

[39] Pine AS. Self-, N2-, O2, H2, Ar, and He broadening in the nu3 band Q branch of CH4. J Chem Phys 1992; 97:773-785.

[40] Pine AS. N2 and Ar broadening and line mixing in the P and R branches of the nu3 band of CH4. J Quant Spectrosc Radiat Transfer 1997; 57:157-176.

[41] Pine AS, Gabard T. Speed-dependent broadening and line mixing in CH4 perturbed by Ar and N2 from multispectrum fits. J Quant Spectrosc Radiat Transfer 2000; 66:69-92.

[42] Pine AS, Gabard T. Multispectrum fits for line mixing in the nu3 band Q branch of methane. J Mol Spectrosc 2003; 217:105-114.

[43] Varanasi P, Chudamani S. Measurements of collision-broadened line widths in the nu4-fundamental band of 12CH4 at low temperatures. J Quant Spectrosc Radiat Transfer 1989; 41:335-343.

[44] Walker HC, Phillips WJ. The collision half-width for the R(0) line of the nu3 band of methane. J Appl Phys 1983; 54:4729-4733.

[45] Millot G, Lavorel B, Steinfeld J. Collisional broadening, line shifting, and line mixing in the stimulated Raman 2nu2 Q branch of CH4. J Chem Phys 1991; 95:7938-7946.

[46] Pieroni D, Nguyen-Van-Thanh, Brodbeck C, Claveau C, Valentin A, Hartmann J-M, Gabard T, Champion J-P, Bermejo D, Domenech J-L. Experimental and theoretical study of line mixing in methane spectra I. The N2-broadened nu3 band at room temperature. J Chem Phys 1999; 110:7717-7732.

[47] Pieroni D, Nguyen-Van-Thanh, Brodbeck C, Hartmann J-M, Gabard T, Champion J-P, Bermejo D, Domenech J-L, Claveau C, Valentin A. Experimental and theoretical study of line mixing in methane spectra. IV. Influence of the temperature and of the band. J Chem Phys 2000; 113:5776-5783.

[48] Pieroni D, Hartmann JM, Camy-Peyret C, Jeseck P, Payan S. Influence of line mixing on absorption by CH4 in atmospheric balloon-borne spectra near 3.3 [mu]m. J Quant Spectrosc Radiat Transfer 2001; 68:117-133.

[49] Benner DC, Rinsland CP, Malathy Devi V, Smith MAH, Atkins D. A multispectrum nonlinear least squares fitting technique. J Quant Spectrosc Radiat Transfer 1995; 53:705-721.

[50] Smith MAH, Benner DC, Predoi-Cross A, Malathy Devi V. Multispectrum analysis of 12CH4 in the nu4 spectral region: II. Self-broadened widths, pressure-induced shifts, temperature dependences and line mixing. Can J Phys 2008;in preparation.

[51] Malathy Devi V, Benner DC, Smith MAH, Rinsland CP, Sharpe SW, Sams RL. A multispectrum analysis of the 2nu2 spectral region of H12C14N: Intensities, broadening and pressure-shift coefficients. J Quant Spectrosc Radiat Transfer 2004; 87:339-366.

[52] Mantz AW, Malathy Devi V, Benner DC, Smith MAH, Predoi-Cross A, Dulick M. A multispectrum analysis of widths and shifts in the 2010 to 2260 cm-1 region of 12C16O broadened by helium at temperatures between 80 and 297 K. J Mol Struct 2005; 742:99-110.

[53] Rothman LS, Jacquemart D, Barbe A, Benner DC, Birk M, Brown LR, Carleer MR, Chackerian C, Chance K, Coudert LH, Dana V, Malathy Devi V, Flaud J-M, Gamache RR, Goldman A, Hartmann J-M, Jucks KW, Maki AG, Mandin J-Y, Massie ST, Orphal J, Perrin A, Rinsland CP, Smith MAH, Tennyson J, Tolchenov RN, Toth RA, Vander Auwera J, Varanasi P, Wagner G. The HITRAN 2004 molecular spectroscopic database. J Quant Spectrosc Radiat Transfer 2005; 96:139-204.

[54] Levy A, Lacome N, Chackerian C. Collisional line mixing. In: Narahari Rao K, Weber A, editors. Spectroscopy of the Earth's Atmosphere and Interstellar Medium. Boston, MA: Academic Press, 1992: 261-337.

[55] Brown LR, Benner DC, Champion JP, Malathy Devi V, Fejard L, Gamache RR, Gabard T, Hilico JC, Lavorel B, Loete M, Mellau GCh, Nikitin A, Pine AS, Predoi-Cross A, Rinsland CP, Robert O, Sams

RL, Smith MAH, Tashkun SA, Tyuterev VG. Methane line parameters in HITRAN. J Quant Spectrosc Radiat Transfer 2003; 82:219-238.

[56] Rosenkranz PW. Shape of the 5 mm oxygen band in the atmosphere. IEEE Trans Antennas Propag 1975; AP-23:498-506.

[57] Predoi-Cross A, Brown LR, Malathy Devi V, Brawley-Tremblay M, Benner DC. Multispectrum analysis of 12CH4 from 4100 to 4635 cm-1: I. Self-broadening coefficients (widths and shifts). J Mol Spectrosc 2005; 232:231-246.

Table(s)

Table 1
Summary of experimental conditions of the CH_4 spectra

Temperature (K)	Gas Mixture	CH_4 Volume Mixing Ratio	Path (m)	Pressure Range (torr)	Number of Spectra
294.5 to 295.9	CH_4	1.0	0.00958	7.0 - 453.3	5
299.8	CH_4	1.0	0.050	0.90	1*
313.1 to 313.7	CH_4 in Air	0.011	0.050	200.0 - 550.1	5*
303.5	CH_4	1.0	0.250	0.73	1
299.5	CH_4 in Air	0.011	0.250	50.2 - 425.6	4*
295.8	CH_4	1.0	1.50	1.18	1*
297.4 to 297.5	CH_4 in Air	0.0272 - 0.0275	1.50	199.6 - 425.0	4*
275.1	CH_4 in Air	0.007	0.500	100.7 - 300.8	3*
257.6 to 256.9	CH_4 in Air	0.0042	0.500	141.1 - 340.1	3*
240.1 to 239.7	CH_4 in Air	0.0043	0.500	140.6 - 338.3	3*
223.1 to 222.8	CH_4 in Air	0.0042 - 0.0044	0.500	140.9 - 340.7	3*
211.6 to 210.2	CH_4 in Air	0.0042 - 0.0044	0.500	140.1 - 335.7	4*
272.5	CH_4	1.0	0.500	301.0	1
272.5 to 272.4	CH_4 in Air	0.33	0.500	177.0 - 452.8	3
254.4 to 253.9	CH_4	1.0	0.500	209.0 - 645.0	3
254.0	CH_4	1.0	0.500	11.0	1
253.8	CH_4 in Air	0.304	0.500	229.1 - 509.2	2
252.9 to 250.5	CH_4 in Air	0.16 - 0.30	0.500	140.2 - 520.1	5
240.7 to 240.6	CH_4 in Air	0.30 - 0.35	0.500	99.2 - 328.2	3
232.7 to 232.6	CH_4	1.0	0.500	128.5 - 370.5	3
232.6	CH_4 in Air	0.31	0.500	418.6	1
225.9	CH_4	1.0	0.500	643.0	1

Note: 760 torr = 1 atm = 101.325 kPa.

* Spectra previously analyzed in Ref. [1].

Table(s)

Table 2
Mean air-broadened half width and pressure-induced shift coefficients and their temperature dependences for allowed P and R transitions in the ν_4 band of $^{12}CH_4$

|m|	Species	Widths and std. dev.[a]	n_1 and std. dev.[b]	Shifts and std. dev.[a]	$\delta' \times 10^4$ and std. dev.[c]	# lines
1	A	0.0547(0)	0.70(0)	-0.0027(0)	0.16(0)	1
2	F	0.0625(0)	0.82(0)	-0.0014(0)	0.12(0)	1
3	E	0.0560(0)	0.80(0)	-0.0016(0)	0.16(0)	1
3	A	0.0608(0)	0.77(0)	-0.0029(0)	0.23(0)	1
3	F	0.0659(9)	0.84(1)	-0.0020(4)	0.16(11)	2
4	E	0.0583(0)	0.77(0)	-0.0034(0)	0.18(0)	1
4	A	0.0609(38)	0.78(2)	-0.0021(6)	0.06(12)	2
4	F	0.0656(24)	0.81(5)	-0.0023(9)	0.18(9)	4
5	E	0.0541(0)	0.74(0)	-0.0022(0)	0.09(0)	1
5	A	0.0593(0)	0.81(0)	-0.0020(0)	0.25(0)	1
5	F	0.0640(22)	0.81(3)	-0.0022(6)	0.11(9)	5
6	E	0.0562(38)	0.73(1)	-0.0022(4)	0.17(13)	2
6	A	0.0601(0)	0.75(0)	-0.0027(0)	0.21(0)	1
6	F	0.0628(18)	0.78(1)	-0.0026(4)	0.17(6)	4
7	E	0.0542(0)	0.72(0)	-0.0028(0)	0.18(0)	1
7	A	0.0577(7)	0.75(1)	-0.0024(8)	0.14(6)	3
7	F	0.0614(18)	0.80(3)	-0.0027(11)	0.12(6)	7
8	E	0.0482(53)	0.72(10)	-0.0029(7)	0.15(3)	3
8	A	0.0536(8)	0.68(3)	-0.0031(1)	0.18(3)	2
8	F	0.0589(25)	0.79(8)	-0.0025(7)	0.16(6)	8
9	E	0.0494(31)	0.75(16)	-0.0029(9)	0.19(11)	3
9	A	0.0547(54)	0.78(15)	-0.0038(19)	0.06(19)	3
9	F	0.0561(29)	0.80(10)	-0.0028(6)	0.19(7)	9

Standard deviations are given in parentheses in units of the last digit quoted.
[a] Widths and shifts correspond to half width and pressure-induced shift coefficients. The units are cm^{-1} atm^{-1} at 296 K.
[b] The temperature dependence exponents of half widths (n_1) are unitless.
[c] The temperature dependence coefficients of air-shifts (δ') are in cm^{-1} atm^{-1} K^{-1}.

Table(s)

Table 3
Off-diagonal relaxation matrix element (ORME) coefficients measured for air-broadening in the ν_4 band of $^{12}CH_4$

Mixing pair(s)	Assignments	$\nu(cm^{-1})$	ORME Coefficients (cm^{-1} atm^{-1} at 296 K)
P(18) F	17F2 10←18F1 4 17F1 9←18F2 5	1159.8003 1160.3022	0.0336(12)
P(17) F	16F2 9←17F1 5 16F1 9←17F2 4	1170.4309 1171.5078	0.0384(10)
P(16) F	15F1 9←16F2 4 15F2 8←16F1 4	1180.9714 1182.1047	0.0300(5)
P(16) F	15F2 9←16F1 3 15F1 10←16F2 3	1190.2366 1191.4300	0.0138(8)
P(15) E P(16) E	15E 6←16E 3 16E 7←17E 2	1181.5285 1181.7764	0.0049(3)
P(15) F	14F1 8←15F2 4 14F2 8←15F1 4	1191.4770 1192.0694	0.0304(2)
P(15) A	14A1 3←15A2 2 14A2 3←15A1 1	1190.9732 1192.8280	0.0302(4)
P(14) F	13F1 7←14F2 4 13F2 8←14F1 3	1201.1321 1202.4211	0.0264(2)
P(14(F)	13F1 8←14F2 3 13F2 9←14F1 2	1207.8332 1210.7839	0.0152(5)
P(13) F	12F2 7←13F1 4 12F1 7←13F2 3	1210.6728 1211.9958	0.0329(2)
P(13) F	12F1 8←13F2 2 12F2 8←13F1 3	1217.6267 1218.6270	0.0073(1)
P(12) F	11F2 6←12F1 3 11F1 7←12F2 3	1220.1905 1220.8588	0.0243(1)
P(12) F	11F2 7←12F1 2 11F1 9←12F2 1	1229.4575 1230.0849	0.0031(0)
P(12) A	11A2 2←12A1 2 11A1 3←12A2 1	1219.6488 1221.8799	0.0261(1)
P(11) F	10F2 6←11F1 3 10F1 6←11F2 3	1228.7926 1230.2891	0.0287(1)
P(10)F	9F1 5←10F2 3 9F2 6←10F1 2	1238.2721 1238.7119	0.0225(1)
P(12) F P(11) F	11F2 8←12F1 1 10F1 7←11F2 2	1235.9535 1236.4262	0.0019(0)
P(12)A P(11)A	11A2 3←12A1 1 10A1 3←11A2 1	1236.0086 1237.0204	0.0056(0)
P(12)E P(11)E	11E 6←12E 1 10E 5←11E 1	1235.9249 1236.0293	0.0009(1)
P(9) A	8A1 2←9A2 1 8A2 2←9A1 1	1245.2197 1247.8232	0.0235(1)
P(9) F	8F1 5←9F2 2 8F2 5←9F1 3	1245.7692 1246.4526	0.0175(0)

P(8) F	7F1 5←8F2 2 7F2 4←8F1 2	1253.3491 1255.0003	0.0257(1)
P(8) F	7F1 5←8F2 2 7F1 6←8F2 1	1253.3491 1256.6018	0.0015(1)
P(7) F	6F2 4←7F1 2 6F1 4←7F2 2	1260.8111 1262.2285	0.0100(1)
P(6) F	5F2 4←6F1 1 5F1 3←6F2 2	1268.3678 1268.9763	0.0101(1)
P(6) A	5A2 2←6A1 1 5A1 1←6A2 1	1267.8224 1270.7851	0.0136(1)
P(5) F	4F2 3←5F1 2 4F1 3←5F2 1	1275.0417 1276.8444	0.0067(0)
P(4) F	3F1 3←4F2 1 3F2 2←4F1 1	1281.6106 1282.9842	0.0039(1)
P(3) F	2F1 2←3F2 1 2F2 2←3F1 1	1288.4571 1288.9510	0.0036(0)
R(3) F	4F1 1←3F2 1 4F2 1←3F1 1	1327.2568 1327.4098	0.0058(0)
R(4) F	5F1 1←4F2 1 5F2 1←4F1 1	1332.0853 1332.5468	0.0071(0)
R(5) F	6F2 1←5F1 2 6F2 2←5F1 1	1336.9599 1337.8238	0.0080(1)
R(5) F	6F2 1←5F1 2 6F1 1←5F2 1	1336.9599 1337.5950	0.0050(1)
R(6) A	7A2 1←6A1 1 7A1 1←6A2 1	1341.6220 1342.6545	0.0198(0)
R(6) F	7F2 1←6F1 1 7F1 1←6F2 2	1341.7781 1341.9590	0.0108(0)
R(7) F	8F2 1←7F1 2 8F1 2←7F2 1	1346.3301 1347.9215	0.0101(0)
R(7) F	8F1 1←7F2 2 8F1 2←7F2 1	1346.9396 1347.9215	0.0144(1)
R(7) F	8F1 1←7F2 2 8F2 2←7F1 1	1346.7396 1348.0417	0.0018(0)
R(8) F	9F1 1←8F2 2 9F2 1←8F1 2	1350.9170 1351.3855	0.0143(1)
R(8) F	9F1 1←8F2 2 9F2 2←8F1 1	1350.9170 1353.0749	0.0118(5)
R(8) E	9E 1←8E 2 9E 2←8E 1	1351.0234 1353.0258	0.0136(7)
R(9) A	10A1 1←9A2 1 10A2 1←9A1 1	1355.3441 1356.0536	0.0221(1)
R(9) F	10F1 1←9F2 2 10F2 1←9F1 3	1355.4730 1355.6393	0.0144(1)
R(9) F	10F1 1←9F2 2 10F2 2←9F1 2	1355.4730 1356.4868	0.0079(2)
R(10) F	11F1 1←10F2 3 11F2 1←10F1 2	1359.8229 1360.1572	0.0182(1)
R(10) F	11F1 1←10F2 3 11F1 2←10F2 2	1359.8229 1361.3611	0.0034(0)

R(11) F	12F2 1←11F1 3 12F1 1←11F2 3	1364.2012 1364.5391	0.0229(1)
R(12) F	13F1 2←12F2 2 13F1 3←12F2 1	1369.5495 1370.8559	0.0103(2)
R(13) F	14F2 1←13F1 4 14F1 1←13F2 3	1372.7749 1373.0266	0.0249(2)
R(13) F	14F2 1←13F1 4 14F2 2←13F1 3	1372.7749 1374.1958	0.0063(1)
R(14) F	15F1 1←14F2 4 15F2 1←14F1 3	1377.0073 1377.2466	0.0286(1)
R(15) A	16A1 1←15A2 2 16A2 1←15A1 1	1381.1580 1381.4932	0.0307(1)
R(15) F	16F1 1←15F2 4 16F2 1←15F1 4	1381.2355 1381.3346	0.0266(1)
R(15) F	16F1 1←15F2 4 16F2 2←15F1 3	1381.2355 1382.2457	0.0306(7)
R(16) F	17F1 1←16F2 4 17F2 1←16F1 4	1385.3496 1385.5338	0.0317(2)
R(18) F	19F2 1←18F1 4 19F1 1←18F2 5	1393.6130 1393.6871	0.0286(6)
R(18) A	19A2 1←18A1 2 19A1 1←18A2 2	1393.5545 1393.8075	0.0343(6)

Values in parentheses are standard error in units of the last digit quoted.

Table(s)

Appendix

Measured spectral line parameters for air-broadening in the methane ν_4 band sorted by $|m|$

|m|	ΔJ	vb	J'	C'	n'	J"	C"	n"	Position[a]	Air width[b]	width[c] temp dep	Air shift[b]	shift temp dep[d]
1	R	3	1	A2	1	0	A1	1	1311.43156(1)	0.0547(0)	0.70(0)	-0.0027(0)	0.000016(0)
2	R	3	2	F2	1	1	F1	1	1316.82715(1)	0.0625(0)	0.82(0)	-0.0014(0)	0.000012(0)
3	R	3	3	E	1	2	E	1	1322.15407(1)	0.0560(1)	0.80(0)	-0.0016(0)	0.000016(1)
3	R	3	3	F1	1	2	F2	1	1322.08525(1)	0.0650(0)	0.84(0)	-0.0016(0)	0.000004(1)
3	Q	3	3	F1	3	3	F2	1	1323.51382(6)*	0.0703(3)	0.97(3)	-0.0050(3)	-0.000050(7)
3	P	3	2	A1	1	3	A2	1	1287.81333(1)	0.0608(0)	0.77(0)	-0.0029(0)	0.000023(0)
3	P	3	2	F1	2	3	F2	1	1288.45706(1)	0.0660(0)	0.83(0)	-0.0022(0)	0.000023(0)
3	P	3	2	F2	2	3	F1	1	1288.95103(1)	0.0668(0)	0.84(0)	-0.0023(0)	0.000022(0)
4	R	3	4	A1	1	3	A2	1	1327.07420(0)	0.0582(0)	0.76(0)	-0.0017(0)	-0.000003(0)
4	R	3	4	F1	1	3	F2	1	1327.25683(0)	0.0664(1)	0.80(0)	-0.0013(0)	0.000010(1)
4	R	3	4	F2	1	3	F1	1	1327.40989(1)	0.0668(0)	0.86(0)	-0.0017(0)	0.000031(1)
4	R	3	4	F2	3	3	F1	1	1369.30463(5)*	0.0691(8)	1.47(6)		
4	Q	3	4	E	2	4	E	1	1327.74760(11)*	0.0772(3)	1.52(3)	0.0003(4)	-0.000044(12)
4	P	3	3	A2	1	4	A1	1	1283.45880(0)	0.0636(0)	0.79(0)	-0.0025(0)	0.000014(0)
4	P	3	3	E	2	4	E	1	1282.62455(1)	0.0583(0)	0.77(0)	-0.0034(0)	0.000018(0)
4	P	3	3	F1	3	4	F2	1	1281.61059(0)	0.0621(0)	0.75(0)	-0.0030(0)	0.000015(0)
4	P	3	3	F2	2	4	F1	1	1282.98416(1)	0.0672(0)	0.83(0)	-0.0031(0)	0.000017(0)
5	R	3	5	A2	1	4	A1	1	1332.72114(0)	0.0593(0)	0.81(0)	-0.0020(0)	0.000025(0)
5	R	3	5	A2	2	4	A1	1	1382.99403(2)*	0.0785(2)			
5	R	3	5	E	1	4	E	1	1332.42483(1)	0.0541(0)	0.74(0)	-0.0022(0)	0.000009(1)
5	R	3	5	F1	1	4	F2	1	1332.08528(0)	0.0621(0)	0.77(0)	-0.0014(0)	0.000003(0)
5	R	3	5	F2	1	4	F1	1	1332.54677(0)	0.0669(0)	0.82(0)	-0.0019(0)	0.000001(1)
5	Q	3	5	F1	3	5	F2	1	1331.78510(2)*	0.0693(2)	1.90(2)	-0.0022(1)	0.000022(6)
5	Q	3	5	F1	4	5	F2	1	1334.19433(6)*	0.0591(6)			
5	Q	3	5	F2	4	5	F1	2	1331.17033(9)*	0.0649(10)	1.21(10)		
5	Q	3	5	F2	4	5	F1	1	1331.18482(4)*	0.0713(4)	1.21(4)	-0.0053(3)	0.000046(9)
5	P	3	4	E	1	5	E	1	1252.23842(3)*	0.0756(4)	1.22(3)	-0.0031(4)	-0.000008(9)
5	P	3	4	F1	6	5	F2	4	1267.21035(11)	0.0631(5)	1.33(8)	-0.0024(5)	-0.000031(22)
5	P	3	4	F1	3	5	F2	1	1276.84437(1)	0.0657(0)	0.84(0)	-0.0027(0)	0.000018(1)
5	P	3	4	F2	2	5	F1	2	1251.86827(7)*	0.0744(6)	0.90(4)		
5	P	3	4	F2	3	5	F1	2	1275.04173(1)	0.0620(0)	0.78(0)	-0.0024(0)	0.000015(0)
5	P	3	4	F2	4	5	F1	1	1277.47337(1)	0.0634(0)	0.82(0)	-0.0027(0)	0.000019(0)
6	R	3	6	E	1	5	E	1	1337.05908(1)	0.0535(0)	0.72(0)	-0.0019(0)	0.000007(1)
6	R	3	6	F1	1	5	F2	1	1337.59498(1)	0.0639(0)	0.79(0)	-0.0022(0)	0.000013(1)
6	R	3	6	F2	2	5	F1	1	1337.82381(1)	0.0605(0)	0.77(0)	-0.0023(0)	0.000010(1)
6	R	3	6	F2	4	5	F1	1	1396.86559(4)*	0.0765(5)	0.98(3)	-0.0062(5)	0.000032(11)
6	Q	3	6	A1	2	6	A2	1	1336.56186(1)*	0.0682(1)	0.97(1)	-0.0032(1)	0.000002(3)
6	R	3	6	F2	1	5	F1	2	1336.95994(1)*	0.0613(0)	0.77(0)	-0.0014(0)	0.000002(1)
6	Q	3	6	E	3	6	E	1	1334.90664(3)*	0.0733(2)	1.05(2)	-0.0037(2)	-0.000002(4)
6	Q	3	6	F1	4	6	F2	2	1335.45687(5)*	0.0684(5)	1.02(4)		
6	Q	3	6	F1	4	6	F2	1	1335.47787(2)*	0.0674(2)	1.07(1)	-0.0054(1)	
6	Q	3	6	F2	4	6	F1	1	1334.04853(5)*	0.0634(4)	1.06(3)	-0.0046(4)	0.000010(9)
6	P	3	5	A1	1	6	A2	1	1270.78509(0)	0.0601(0)	0.75(0)	-0.0027(0)	0.000021(0)
6	P	3	5	A2	1	6	A1	1	1217.54864(8)*	0.0722(7)	1.08(6)	0.0034(7)	0.000031(17)
6	P	3	5	E	3	6	E	1	1271.58947(1)	0.0589(0)	0.73(0)	-0.0024(0)	0.000026(1)
6	P	3	5	F1	2	6	F2	2	1240.56954(3)*	0.0676(2)	1.16(2)	-0.0022(2)	0.000003(7)
6	P	3	5	F1	3	6	F2	2	1268.97630(1)	0.0643(0)	0.79(0)	-0.0030(0)	0.000023(1)
6	P	3	5	F1	4	6	F2	1	1271.40695(1)	0.0623(0)	0.77(0)	-0.0028(0)	0.000020(1)
6	P	3	5	F2	2	6	F1	1	1239.97057(5)*	0.0714(5)	1.04(5)	0.0020(5)	0.000032(15)
6	P	3	5	F2	4	6	F1	1	1268.36784(1)	0.0622(0)	0.78(0)	-0.0029(0)	0.000014(1)
7	R	3	7	A1	1	6	A2	1	1342.65445(0)	0.0571(0)		-0.0022(0)	0.000021(1)
7	R	3	7	A1	2	6	A2	1	1376.80611(2)*	0.0683(1)	1.07(1)	-0.0017(1)	0.000013(2)
7	R	3	7	A2	1	6	A1	1	1341.62204(0)	0.0584(0)	0.75(0)	-0.0017(0)	0.000010(0)
7	R	3	7	E	1	6	E	1	1342.94542(1)	0.0542(0)	0.72(0)	-0.0028(0)	0.000018(1)
7	R	3	7	F1	1	6	F2	2	1341.95897(1)	0.0642(0)	0.78(0)	-0.0017(0)	0.000017(0)
7	R	3	7	F1	2	6	F2	1	1342.87317(1)	0.0616(0)	0.76(0)	-0.0030(0)	0.000020(1)
7	R	3	7	F1	4	6	F2	1	1377.72186(4)*	0.0671(2)		-0.0081(3)	0.000043(6)
7	R	3	7	F1	5	6	F2	2	1410.23866(7)*	0.0687(6)	0.94(6)	-0.0031(7)	0.000097(16)
7	R	3	7	F1	5	6	F2	1	1410.26073(5)*	0.0768(5)	0.90(4)	-0.0082(6)	-0.000012(14)
7	R	3	7	F2	1	6	F1	1	1341.77807(1)	0.0615(0)	0.80(0)	-0.0009(0)	0.000002(2)
7	R	3	7	F2	4	6	F1	1	1411.86405(8)*	0.0667(7)	0.85(7)	-0.0022(7)	-0.000005(18)
7	Q	3	7	A1	1	7	A2	1	1269.42019(4)*	0.0662(3)	0.98(2)	-0.0005(3)	-0.000002(6)
7	Q	3	7	E	1	7	E	1	1269.68942(10)*	0.0853(11)			
7	Q	3	7	E	3	7	E	1	1337.44032(4)*	0.0834(9)			
7	Q	3	7	F1	2	7	F2	2	1269.62485(6)*	0.0665(6)			
7	Q	3	7	F2	4	7	F1	1	1338.68219(2)*	0.0686(1)	1.12(1)	-0.0057(1)	0.000040(3)
7	P	3	6	A1	2	7	A2	1	1263.32741(1)	0.0577(0)	0.74(0)	-0.0033(0)	0.000011(1)

7	P	3	6	E	3	7	E	1	1261.64995(1)	0.0466(0)	0.70(0)	-0.0051(0)	0.000021(1)
7	P	3	6	E	2	7	E	1	1228.11450(4)*	0.0730(3)	1.03(3)	-0.0003(3)	-0.000001(8)
7	P	3	6	F1	2	7	F2	2	1228.30451(2)*	0.0673(2)	1.07(2)	0.0014(2)	0.000001(4)
7	P	3	6	F1	3	7	F2	2	1231.77481(7)*	0.0678(5)	0.97(4)		
7	P	3	6	F1	4	7	F2	2	1262.22848(1)	0.0632(0)	0.81(0)	-0.0037(0)	0.000015(1)
7	P	3	6	F1	5	7	F2	1	1265.37370(1)	0.0605(0)	0.85(0)	-0.0024(0)	0.000012(1)
7	P	3	6	F2	2	7	F1	2	1201.77017(5)*	0.0713(6)	1.08(5)		
7	P	3	6	F2	3	7	F1	2	1232.40829(4)*	0.0667(5)	0.89(4)		
7	P	3	6	F2	4	7	F1	2	1260.81110(1)	0.0604(0)	0.83(0)	-0.0032(0)	0.000012(1)
7	P	3	6	F2	5	7	F1	1	1265.68666(1)	0.0586(0)	0.80(0)	-0.0038(0)	0.000006(1)
8	R	3	8	A1	1	7	A2	1	1347.05431(1)	0.0541(0)	0.70(0)	-0.0030(0)	0.000016(0)
8	R	3	8	A1	2	7	A2	1	1422.93849(2)*	0.0715(1)	1.02(1)	-0.0072(1)	0.000048(3)
8	R	3	8	E	1	7	E	1	1346.57552(1)	0.0433(0)	0.61(0)	-0.0022(0)	0.000013(0)
8	R	3	8	E	4	7	E	1	1427.63071(5)*	0.0756(4)			
8	R	3	8	F1	1	7	F2	2	1346.73962(1)	0.0628(0)	0.77(0)	-0.0019(0)	0.000013(0)
8	R	3	8	F1	2	7	F2	1	1347.92147(1)	0.0590(0)	0.75(0)	-0.0028(0)	0.000014(0)
8	R	3	8	F1	5	7	F2	2	1423.46990(4)*	0.0677(3)	0.91(3)	-0.0058(3)	0.000092(9)
8	R	3	8	F1	5	7	F2	1	1423.50784(5)*	0.0745(4)	0.83(3)	-0.0036(4)	0.000041(10)
8	R	3	8	F2	1	7	F1	2	1346.33011(1)	0.0595(0)	0.76(0)	-0.0013(0)	0.000003(0)
8	R	3	8	F2	2	7	F1	1	1348.04161(1)	0.0555(0)	0.70(0)	-0.0029(0)	0.000018(0)
8	R	3	8	F2	4	7	F1	1	1387.63660(4)*	0.0721(3)	0.61(3)	-0.0092(3)	-0.000020(7)
8	Q	3	8	E	4	8	E	1	1344.06467(6)*	0.0635(3)		-0.0056(2)	
8	Q	3	8	F1	2	8	F2	1	1264.26235(3)*	0.0603(4)	1.12(4)		
8	Q	3	8	F2	6	8	F1	2	1343.62694(9)*	0.0621(6)		-0.0006(4)	
8	Q	3	8	F2	6	8	F1	1	1343.69838(6)*	0.0587(3)		-0.0042(3)	
8	P	3	7	A2	2	8	A1	1	1259.88421(1)	0.0530(0)	0.66(0)	-0.0031(0)	0.000020(1)
8	P	3	7	E	1	8	E	2	1186.03846(8)*	0.0704(5)			
8	P	3	7	E	2	8	E	2	1221.37421(3)*	0.0785(4)	1.00(4)		
8	P	3	7	E	3	8	E	2	1253.78914(1)	0.0475(1)	0.78(0)	-0.0035(1)	0.000014(1)
8	P	3	7	E	4	8	E	1	1259.52525(1)	0.0538(1)	0.78(0)	-0.0031(1)	0.000018(1)
8	P	3	7	F1	3	8	F2	1	1216.24012(3)*	0.0668(3)		0.0004(3)	
8	P	3	7	F1	5	8	F2	2	1253.34911(1)	0.0601(0)	0.89(0)	-0.0021(0)	0.000021(1)
8	P	3	7	F1	6	8	F2	1	1256.60182(1)	0.0578(0)	0.82(0)	-0.0032(0)	0.000016(1)
8	P	3	7	F2	2	8	F1	2	1215.94794(3)*	0.0673(2)	0.94(2)	0.0025(2)	-0.000013(5)
8	P	3	7	F2	4	8	F1	2	1255.00032(1)	0.0609(0)	0.91(0)	-0.0027(0)	0.000020(1)
8	P	3	7	F2	5	8	F1	1	1259.66151(1)	0.0557(1)	0.73(0)	-0.0030(0)	0.000020(1)
9	R	3	9	A2	1	8	A1	1	1353.15906(1)	0.0485(0)	0.61(0)	-0.0033(0)	0.000019(0)
9	R	3	9	A2	3	8	A1	1	1439.48753(2)*	0.0620(1)	0.87(1)	-0.0088(1)	0.000036(4)
9	R	3	9	E	1	8	E	2	1351.02355(1)	0.0458(0)	0.65(0)	-0.0019(0)	0.000009(1)
9	R	3	9	E	2	8	E	1	1353.02582(1)	0.0514(0)	0.67(0)	-0.0034(0)	0.000018(1)
9	R	3	9	E	3	8	E	1	1395.55503(3)*	0.0633(3)	0.91(3)	-0.0031(3)	0.000037(7)
9	R	3	9	F1	1	8	F2	2	1350.91695(1)	0.0579(0)	0.75(0)	-0.0013(0)	0.000009(1)
9	R	3	9	F1	2	8	F2	1	1351.80987(1)	0.0539(0)	0.70(0)	-0.0030(0)	0.000019(0)
9	R	3	9	F1	5	8	F2	1	1435.77175(3)*	0.0707(2)	0.99(2)	-0.0072(2)	0.000044(6)
9	R	3	9	F2	1	8	F1	2	1351.38549(1)	0.0585(0)	0.75(0)	-0.0025(0)	0.000011(1)
9	R	3	9	F2	2	8	F1	1	1353.07488(1)	0.0538(0)	0.68(0)	-0.0031(0)	0.000018(1)
9	R	3	9	F2	4	8	F1	1	1395.89646(2)*	0.0619(2)	0.83(2)	-0.0060(2)	0.000024(5)
9	R	3	9	F2	5	8	F1	2	1399.15704(5)*	0.0664(5)	0.90(5)	0.0038(6)	0.000137(13)
9	Q	3	9	A2	1	9	A1	1	1259.05886(4)*	0.0636(5)	1.23(5)		
9	Q	3	9	A2	3	9	A1	1	1345.38700(3)*	0.0643(1)		0.0010(1)	
9	Q	3	9	E	2	9	E	1	1258.96236(7)*	0.0571(7)	1.38(8)		
9	Q	3	9	F1	6	9	F2	1	1347.80154(5)*	0.0550(5)		-0.0049(4)	
9	Q	3	9	F2	2	9	F1	2	1259.00356(6)*	0.0591(6)	0.97(6)		
9	Q	3	9	F2	7	9	F1	1	1347.12615(7)*	0.0447(10)			
9	P	3	8	A1	1	9	A2	1	1169.33582(4)*	0.0713(3)	0.83(4)	0.0035(3)	-0.000011(11)
9	P	3	8	A1	2	9	A2	1	1245.21974(1)	0.0580(0)	0.90(0)	-0.0023(0)	0.000016(1)
9	P	3	8	A2	1	9	A1	1	1203.38610(2)*	0.0680(1)	1.02(1)	0.0016(1)	-0.000016(3)
9	P	3	8	A2	2	9	A1	1	1247.82317(1)	0.0575(1)	0.84(1)	-0.0059(1)	-0.000016(1)
9	P	3	8	E	2	9	E	1	1203.68760(3)*	0.0616(2)	0.93(2)	-0.0006(2)	0.000008(4)
9	P	3	8	E	3	9	E	1	1211.67363(14)*	0.0621(8)	0.75(9)	-0.012(6)	
9	P	3	8	E	4	9	E	1	1250.00112(1)	0.0509(0)	0.93(0)	-0.0034(0)	0.000030(1)
9	P	3	8	F1	3	9	F2	2	1208.69925(4)*	0.0710(3)			
9	P	3	8	F1	4	9	F2	1	1212.16481(15)*	0.0746(13)			
9	P	3	8	F1	5	9	F2	2	1245.76924(1)	0.0586(0)	0.95(0)	-0.0029(0)	0.000018(1)
9	P	3	8	F1	6	9	F2	1	1253.66154(1)	0.0540(1)	0.76(0)	-0.0034(0)	0.000023(1)
9	P	3	8	F2	2	9	F1	3	1170.31097(6)*	0.0715(5)			
9	P	3	8	F2	3	9	F1	2	1203.58543(2)*	0.0601(1)	0.97(1)	0.0015(1)	-0.000014(3)
9	P	3	8	F2	4	9	F1	3	1209.90479(4)*	0.0613(3)	1.07(3)	-0.0029(3)	-0.000012(7)
9	P	3	8	F2	5	9	F1	3	1246.45257(1)	0.0592(0)	0.90(0)	-0.0026(0)	0.000030(1)
9	P	3	8	F2	6	9	F1	2	1249.62669(1)	0.0575(0)	0.90(0)	-0.0029(0)	0.000027(1)
9	P	3	8	F2	7	9	F1	1	1253.85109(1)	0.0511(1)	0.79(0)	-0.0033(0)	0.000014(1)
10	R	3	10	A1	1	9	A2	1	1355.34406(1)	0.0557(0)	0.75(0)	-0.0015(0)	0.000007(1)
10	R	3	10	A2	1	9	A1	1	1356.05362(1)	0.0536(0)	0.74(0)	-0.0024(0)	0.000019(0)
10	R	3	10	A2	2	9	A1	1	1407.59274(2)*	0.0662(1)	1.07(1)	0.0012(1)	-0.000025(3)
10	R	3	10	E	1	9	E	1	1356.59736(1)	0.0475(0)	0.64(0)	-0.0036(0)	0.000024(1)

10	R	3	10	E	3	9	E	1	1409.78357(7)*	0.0738(5)	0.92(5)	-0.0030(6)	0.000029(16)
10	R	3	10	F1	1	9	F2	2	1355.47296(1)	0.0571(0)	0.76(0)	-0.0009(0)	0.000016(1)
10	R	3	10	F1	2	9	F2	1	1358.10651(1)	0.0514(0)	0.69(0)	-0.0035(0)	0.000020(1)
10	R	3	10	F1	8	9	F2	2	1460.70629(17)*	0.0827(16)			
10	R	3	10	F2	1	9	F1	3	1355.63928(1)	0.0586(0)	0.77(0)	-0.0029(0)	0.000013(1)
10	R	3	10	F2	2	9	F1	2	1356.48680(1)	0.0551(0)	0.74(0)	-0.0025(0)	0.000018(1)
10	R	3	10	F2	3	9	F1	1	1358.17221(1)	0.0470(0)	0.65(0)	-0.0041(0)	0.000023(1)
10	R	3	10	F2	5	9	F1	3	1409.03462(6)*	0.0625(8)	0.99(9)		
10	R	3	10	F2	5	9	F1	2	1409.08418(5)*	0.0623(3)	1.07(4)	-0.0069(4)	0.000042(11)
10	R	3	10	F2	7	9	F1	1	1452.69552(4)*	0.0586(3)	1.06(4)	-0.0094(3)	0.000029(9)
10	Q	3	10	A1	3	10	A2	1	1351.82733(16)*	0.0610(12)			
10	Q	3	10	A2	1	10	A1	1	1251.66060(3)*	0.0711(3)			
10	Q	3	10	E	5	10	E	1	1350.86247(34)*	0.0518(15)			
10	Q	3	10	F1	6	10	F2	2	1345.13656(12)*	0.0653(5)		-0.0066(4)	
10	Q	3	10	F2	7	10	F1	2	1348.15263(10)*	0.0593(11)		-0.0032(8)	
10	Q	3	10	F2	7	10	F1	1	1348.22801(9)*	0.0560(6)		-0.0047(5)	
10	P	3	9	A1	1	10	A2	1	1202.24445(8)*	0.0607(9)	1.59(10)		
10	P	3	9	A1	2	10	A2	1	1247.70509(1)	0.0487(1)	0.79(0)	-0.0018(0)	0.000027(1)
10	P	3	9	A2	2	10	A1	1	1198.55851(1)*	0.0647(1)	1.05(1)	-0.0055(1)	0.000031(2)
10	P	3	9	A2	3	10	A1	1	1240.99504(1)	0.0540(0)	0.84(0)	-0.0029(0)	0.000028(1)
10	P	3	9	E	3	10	E	2	1197.01871(9)*	0.0756(4)		0.0003(5)	
10	P	3	9	E	4	10	E	2	1238.02243(1)	0.0358(0)	0.68(1)	-0.0049(0)	0.000026(1)
10	P	3	9	E	5	10	E	1	1247.90506(1)	0.0450(1)	0.83(1)	-0.0036(1)	0.000020(2)
10	P	3	9	F1	3	10	F2	2	1190.87640(2)*	0.0566(1)	0.83(2)	0.0006(1)	0.000017(4)
10	P	3	9	F1	4	10	F2	3	1201.40568(8)*	0.0675(10)	0.78(11)		
10	P	3	9	F1	5	10	F2	3	1237.27214(1)	0.0562(0)	0.93(0)	-0.0034(0)	0.000015(1)
10	P	3	9	F1	6	10	F2	2	1243.35187(1)	0.0528(0)	0.83(0)	-0.0041(0)	0.000025(1)
10	P	3	9	F1	7	10	F2	1	1247.84293(1)	0.0452(2)	0.93(1)	-0.0032(1)	0.000068(3)
10	P	3	9	F2	3	10	F1	1	1190.74553(2)*	0.0608(2)	0.76(2)	0.0021(2)	0.000007(4)
10	P	3	9	F2	4	10	F1	2	1197.37086(6)*	0.0674(4)	0.88(4)		
10	P	3	9	F2	4	10	F1	1	1197.44498(8)*	0.0575(8)	0.83(9)		
10	P	3	9	F2	6	10	F1	2	1238.71192(1)	0.0565(0)	0.93(0)	-0.0030(0)	0.000027(1)
10	P	3	9	F2	7	10	F1	1	1242.65885(1)	0.0565(0)	0.87(0)	-0.0022(0)	0.000032(1)
11	R	3	11	A1	2	10	A2	1	1412.62611(1)*	0.0521(1)	0.91(1)	-0.0056(1)	0.000009(2)
11	R	3	11	A1	3	10	A2	1	1461.91353(7)*	0.0658(4)	1.02(5)	-0.0080(4)	0.000016(13)
11	R	3	11	A2	1	10	A1	1	1360.61838(1)	0.0529(0)	0.6(0)	-0.0025(0)	0.000021(1)
11	R	3	11	A2	2	10	A1	1	1459.56965(2)*	0.0675(1)	0.99(1)	-0.0080(1)	0.000035(4)
11	R	3	11	E	1	10	E	2	1360.00011(1)	0.0334(0)	0.45(1)	-0.0023(0)	0.000014(1)
11	R	3	11	E	3	10	E	1	1413.27259(3)*	0.0564(2)	1.01(2)	-0.0077(2)	0.000027(4)
11	R	3	11	F1	1	10	F2	3	1359.82294(1)	0.0558(0)	0.70(1)	-0.0014(0)	0.000020(2)
11	R	3	11	F1	2	10	F2	2	1361.36115(1)	0.0509(0)	0.62(1)	-0.0036(0)	0.000028(1)
11	R	3	11	F1	5	10	F2	1	1413.02995(2)*	0.0534(1)	0.93(1)	-0.0070(1)	0.000039(3)
11	R	3	11	F1	7	10	F2	2	1460.80570(6)*	0.0710(4)	1.06(4)	-0.0034(4)	0.000065(12)
11	R	3	11	F1	8	10	F2	2	1465.37027(10)*	0.0575(5)	1.04(7)	-0.0074(5)	0.000006(16)
11	R	3	11	F1	8	10	F2	1	1465.48791(12)*	0.0623(6)	0.98(7)	-0.0091(6)	0.000007(18)
11	R	3	11	F2	1	10	F1	2	1360.15721(1)	0.0571(0)	0.69(1)	-0.0019(0)	0.000008(2)
11	R	3	11	F2	2	10	F1	1	1361.16783(1)	0.0557(0)	0.66(1)	-0.0035(0)	0.000008(1)
11	R	3	11	F2	6	10	F1	1	1460.13805(5)*	0.0660(3)	1.08(4)	-0.0052(4)	0.000057(10)
11	Q	3	11	A1	1	11	A2	1	1248.33108(4)*	0.0543(4)	1.04(4)		
11	Q	3	11	E	5	11	E	1	1351.18850(16)*	0.0680(9)			
11	Q	3	11	F1	3	11	F2	2	1248.35855(7)*	0.0629(7)	1.28(7)		
11	Q	3	11	F1	4	11	F2	1	1289.72097(1)	0.0439(1)	0.72(1)	-0.0023(1)	0.000029(1)
11	Q	3	11	F1	9	11	F2	1	1355.24351(8)*	0.0443(6)			
11	Q	3	11	F2	3	11	F1	1	1289.68389(1)	0.0422(0)	0.69(1)	-0.0032(1)	0.000027(1)
11	P	3	10	A1	2	11	A2	1	1177.87133(1)*	0.0508(1)	0.83(1)	-0.0019(1)	0.000026(3)
11	P	3	6	A1	1	7	A2	1	1228.81003(1)*	0.0769(5)	1.21(5)		
11	P	3	10	A1	3	11	A2	1	1237.02047(1)	0.0455(0)	0.72(0)	-0.0026(0)	0.000028(1)
11	P	3	10	E	2	11	E	1	1177.74271(4)*	0.0561(3)	0.93(4)	0.0010(3)	-0.000009(9)
11	P	3	10	E	3	11	E	2	1190.54214(13)*	0.0787(9)	0.74(9)	0.0074(9)	0.000093(29)
11	P	3	10	E	3	11	E	1	1190.69547(16)*	0.0694(12)	1.14(12)		
11	P	3	10	E	4	11	E	2	1229.29683(1)	0.0367(0)	0.86(1)	-0.0036(0)	0.000022(1)
11	P	3	10	E	5	11	E	1	1236.02927(1)	0.0473(1)	0.88(2)	-0.0043(1)	0.000066(4)
11	P	3	10	F1	3	11	F2	2	1177.78622(2)*	0.0530(2)	0.86(3)	0.0002(2)	0.000004(6)
11	P	3	10	F1	4	11	F2	3	1185.06207(6)*	0.0697(3)	0.85(4)	0.0024(3)	0.000026(10)
11	P	3	10	F1	7	11	F2	2	1236.42619(1)	0.0518(0)	0.88(1)	-0.0031(0)	0.000024(2)
11	P	3	10	F1	8	11	F2	1	1241.86320(1)	0.0440(0)	0.82(1)	-0.0025(0)	0.000034(1)
11	P	3	10	F2	4	11	F1	2	1185.68946(3)*	0.0565(2)	0.99(2)	-0.0032(2)	0.000003(7)
11	P	3	10	F2	5	11	F1	2	1189.93252(5)*	0.0625(3)	0.89(4)	-0.0055(3)	0.000053(10)
11	P	3	10	F2	6	11	F1	3	1228.79259(1)	0.0543(0)	0.93(1)	-0.0027(0)	0.000015(1)
11	P	3	10	F2	7	11	F1	2	1233.45542(1)	0.0538(0)	0.97(0)	-0.0024(0)	0.000023(1)
11	P	3	10	F2	8	11	F1	1	1241.94890(1)	0.0427(0)	0.72(1)	-0.0036(0)	0.000020(1)
12	R	3	12	A1	1	11	A2	1	1366.19325(1)	0.0418(0)	0.72(1)	-0.0039(0)	0.000026(1)
12	R	3	12	A1	2	11	A2	1	1428.79093(3)*	0.0682(2)	1.03(2)	-0.0053(2)	0.000012(7)
12	R	3	12	E	1	11	E	2	1364.29879(1)	0.0356(1)	0.79(1)	-0.0014(0)	0.000007(2)
12	R	3	12	E	2	11	E	1	1365.94372(1)	0.0461(1)	0.92(1)	-0.0039(1)	0.000046(2)

12	R	3	12	E	4	11	E	1	1426.31083(6)*	0.0642(2)		-0.0021(3)	
11	Q	3	11	F1	8	11	F2	3	1350.52355(9)	0.0628(4)			
12	R	3	12	F1	1	11	F2	3	1364.53906(1)	0.0529(1)	0.95(1)	-0.0015(1)	0.000028(2)
12	R	3	12	F1	2	11	F2	2	1366.04013(1)	0.0502(1)	0.89(1)	-0.0038(1)	0.000028(2)
12	R	3	12	F1	4	11	F2	1	1420.97791(2)*	0.0484(1)	0.90(1)	-0.0055(1)	0.000029(3)
12	R	3	12	F1	5	11	F2	3	1426.65590(10)*	0.0673(5)			
12	R	3	12	F1	5	11	F2	2	1426.79580(5)*	0.0567(2)		-0.0045(2)	
12	R	3	12	F2	1	11	F1	3	1364.20121(1)	0.0537(1)	0.91(1)	-0.0013(1)	0.000018(2)
12	R	3	12	F2	2	11	F1	2	1365.12639(1)	0.0509(1)	0.86(1)	-0.0017(0)	0.000018(1)
12	R	3	12	F2	5	11	F1	1	1421.29748(2)*	0.0517(1)	0.86(1)	-0.0078(1)	0.000041(3)
12	Q	3	12	A1	3	12	A2	1	1351.49734(8)*	0.0629(4)			
12	Q	3	12	A2	1	12	A1	1	1286.54374(1)	0.0379(0)	0.68(1)	-0.0035(1)	0.000019(2)
12	Q	3	12	A2	3	12	A1	1	1358.15034(9)*	0.0487(41)			
12	Q	3	12	F1	8	12	F2	3	1352.85050(27)*	0.0668(14)			
12	Q	3	12	F2	4	12	F1	1	1286.56359(1)	0.0397(1)	0.57(2)	-0.0028(1)	0.000043(3)
12	Q	3	12	F2	9	12	F1	1	1358.64391(8)*	0.0421(4)			
12	P	3	11	A1	2	12	A2	1	1172.59247(3)*	0.0663(2)	1.23(3)	-0.0001(3)	-0.000029(11)
12	P	3	11	A1	3	12	A1	2	1221.87989(1)	0.0520(0)	1.02(0)	-0.0030(0)	0.000033(1)
12	P	3	11	A2	2	12	A2	1	1219.64879(1)	0.0541(0)	1.04(0)	-0.0024(0)	0.000013(1)
12	P	3	11	A2	3	12	A1	1	1236.00855(1)	0.0375(1)	0.67(1)	-0.0039(1)	0.000007(2)
12	P	3	11	E	3	12	E	2	1173.33050(4)*	0.0585(3)	0.93(5)	-0.0039(3)	-0.000032(11)
12	P	3	11	E	4	12	E	2	1180.82697(14)*	0.0583(7)		-0.0091(8)	
12	P	3	11	E	5	12	E	2	1226.08177(1)	0.0466(0)	0.94(1)	-0.0034(0)	0.000031(1)
12	P	3	11	E	6	12	E	1	1235.92492(1)	0.0385(1)	0.90(2)	-0.0022(1)	0.000013(4)
12	P	3	11	F1	4	12	F2	1	1164.56215(4)*	0.0486(2)	0.90(3)	-0.0004(2)	0.000014(7)
12	P	3	11	F1	5	12	F2	2	1173.07439(4)*	0.0547(3)	0.82(5)	0.0002(3)	0.000007(10)
12	P	3	11	F1	6	12	F2	2	1179.35294(5)*	0.0632(4)	0.81(5)	-0.0069(4)	0.000047(12)
12	P	3	11	F1	7	12	F2	3	1220.85979(1)	0.0540(0)	1.07(1)	-0.0033(0)	0.000033(1)
12	P	3	11	F1	8	12	F2	2	1225.53177(1)	0.0536(0)	0.97(1)	-0.0026(0)	0.000021(1)
12	P	3	11	F1	9	12	F2	1	1230.08485(1)	0.0451(0)	0.86(1)	-0.0060(0)	0.000019(2)
12	P	3	11	F2	3	12	F1	2	1164.50491(4)*	0.0527(2)	0.89(4)	0.0006(2)	0.000001(8)
12	P	3	11	F2	6	12	F1	3	1220.19049(1)	0.0542(0)	1.05(1)	-0.0036(0)	0.000006(1)
12	P	3	11	F2	7	12	F1	2	1229.45751(1)	0.0519(0)	0.92(1)	-0.0030(0)	0.000026(1)
12	P	3	11	F2	8	12	F1	1	1235.95353(1)	0.0386(1)	0.73(2)	-0.0024(1)	0.000045(3)
13	R	3	13	A1	2	12	A2	1	1438.03219(4)*	0.0630(2)	1.05(3)	0.0025(3)	-0.000008(8)
13	R	3	13	A2	2	12	A1	1	1373.20430(1)	0.0378(1)		-0.0053(1)	
13	R	3	13	A2	3	12	A1	1	1429.14853(2)*	0.0498(1)	0.95(1)	-0.0084(1)	0.000062(3)
13	R	3	13	A2	4	12	A1	2	1492.56185(9)*	0.0667(5)	1.26(7)	0.0032(4)	
13	R	3	13	A2	4	12	A1	1	1493.06000(11)*	0.0515(4)		-0.0097(5)	
13	R	3	13	E	1	12	E	2	1369.67238(1)	0.0432(0)	0.68(1)	-0.0033(0)	0.000023(1)
13	R	3	13	E	2	12	E	1	1373.18070(2)	0.0387(5)		-0.0031(3)	-0.000002(5)
13	R	3	13	E	3	12	E	1	1428.84223(4)*	0.0483(2)	0.89(4)	-0.0052(2)	0.000020(7)
13	R	3	13	F1	2	12	F2	2	1369.54951(1)	0.0514(0)	0.83(1)	-0.0031(0)	0.000011(2)
13	R	3	13	F1	3	12	F2	1	1370.85592(1)	0.0429(0)	0.68(1)	-0.0038(0)	0.000029(1)
13	R	3	13	F1	5	12	F2	1	1435.94571(8)*	0.0527(4)	1.03(5)	-0.0046(4)	0.000056(12)
13	R	3	13	F1	7	12	F2	2	1482.29492(9)*	0.0674(5)	0.96(6)	-0.0056(5)	0.000019(16)
13	R	3	13	F2	2	12	F1	2	1370.71660(1)	0.0503(0)	0.79(1)	-0.0036(0)	0.000016(1)
13	R	3	13	F2	3	12	F1	1	1373.18855(2)	0.0389(5)			
13	R	3	13	F2	5	12	F1	1	1428.93855(3)*	0.0473(1)	0.83(2)	-0.0068(2)	0.000026(5)
13	R	3	13	F2	6	12	F1	2	1435.09885(6)*	0.0525(3)	0.90(4)	-0.0038(3)	0.000030(10)
13	R	3	13	F2	8	12	F1	2	1483.66899(11)*	0.0623(9)	1.38(12)	-0.0019(9)	0.000131(34)
13	Q	3	13	A1	1	13	A2	1	1233.65099(14)*	0.0915(16)			
13	Q	3	13	F1	4	13	F2	1	1283.21798(2)	0.0364(2)		-0.0034(2)	
13	Q	3	13	F2	4	13	F1	1	1283.20774(2)	0.0347(1)		-0.0037(2)	
13	Q	3	13	F2	10	13	F1	1	1362.11884(10)*	0.0494(7)			
13	P	3	12	A1	2	13	A2	1	1168.26784(3)*	0.0606(2)	1.12(3)	-0.0078(2)	0.000041(8)
13	P	3	12	A1	3	13	A2	1	1216.19950(1)	0.0520(0)	0.94(1)	-0.0025(0)	0.000030(2)
13	P	3	12	A2	3	13	A1	1	1222.64283(1)	0.0497(0)	0.90(1)	-0.0045(0)	0.000010(1)
13	P	3	12	E	5	13	E	2	1211.32963(1)	0.0268(0)	0.73(1)	-0.005(0)	0.000025(1)
13	P	3	12	F1	4	13	F2	2	1160.34870(5)*	0.0552(5)	0.95(8)		
13	P	3	12	F1	5	13	F2	3	1166.18686(16)*	0.0652(12)			
13	P	3	12	F1	5	13	F2	2	1166.33455(16)*	0.0552(10)			
13	P	3	12	F1	6	13	F2	2	1170.05292(12)*	0.0595(6)		-0.0064(6)	
13	P	3	12	F1	7	13	F2	3	1211.99590(1)	0.0541(1)	1.02(1)	-0.0049(1)	0.000031(2)
13	P	3	12	F1	8	13	F2	2	1217.62670(1)	0.0531(0)	0.96(1)	-0.0028(0)	0.000024(1)
13	P	3	12	F1	9	13	F2	1	1229.96461(1)	0.0360(1)	0.82(1)	-0.0028(0)	0.000004(3)
13	P	3	12	F2	5	13	F1	3	1160.69812(6)*	0.0543(3)	0.88(5)	-0.0035(3)	0.000011(11)
13	P	3	12	F2	7	13	F1	4	1210.67278(1)	0.0546(0)	1.02(1)	-0.0028(0)	0.000008(1)
13	P	3	12	F2	8	13	F1	3	1218.62700(1)	0.0505(0)	1.00(1)	-0.0032(0)	0.000019(1)
13	P	3	12	F2	9	13	F1	2	1223.15589(1)	0.0462(0)	0.91(1)	-0.0027(0)	0.000023(1)
13	P	3	12	F2	10	13	F1	1	1223.35630(1)	0.0405(0)	0.82(1)	-0.0029(0)	0.000023(1)
13	P	3	12	F2	10	13	F1	1	1230.00033(1)	0.0366(1)	0.76(2)	-0.0002(1)	0.000029(3)
14	R	3	14	A1	1	13	A2	1	1373.60980(1)	0.0490(1)	0.77(2)	-0.0021(0)	0.000007(4)
14	R	3	14	A1	3	13	A2	1	1492.64948(8)*	0.0622(5)	1.25(8)	-0.0086(5)	-0.00006(19)
14	R	3	14	A2	1	13	A1	1	1375.42330(1)	0.0486(1)	0.69(2)	-0.0041(0)	0.000021(4)

14	R	3	14	A2	2	13	A1	1	1443.18781(3)*	0.0493(2)	1.01(3)	-0.0014(2)	0.000022(6)
14	R	3	14	A2	3	13	A1	1	1494.67586(16)*	0.0686(7)		-0.0096(7)	
14	R	3	14	E	1	13	E	2	1372.90110(1)	0.0244(1)	0.49(4)	-0.0022(0)	0.000022(4)
14	R	3	14	E	2	13	E	1	1375.56660(1)	0.0383(1)	0.64(4)	-0.0044(1)	0.000014(8)
14	R	3	14	E	4	13	E	1	1444.27761(11)*	0.0507(6)	1.64(10)	-0.0086(6)	0.000032(23)
14	R	3	14	F1	1	13	F2	3	1373.02664(1)	0.0512(1)	0.73(3)	-0.0014(1)	0.000026(7)
14	R	3	14	F1	2	13	F2	2	1373.98313(1)	0.0509(1)	0.81(3)	-0.0028(1)	0.000035(7)
14	R	3	14	F1	3	13	F2	1	1378.14660(2)	0.0395(2)	1.49(6)	-0.0012	
14	R	3	14	F2	1	13	F1	4	1372.77487(1)	0.0512(1)	0.76(3)	-0.0013(1)	0.000023(7)
14	R	3	14	F2	2	13	F1	3	1374.19577(1)	0.0487(1)	0.69(3)	-0.0029(0)	0.000030(6)
14	R	3	14	F2	3	13	F1	2	1375.52368(1)	0.0443(1)	0.65(3)	-0.0039(1)	0.000031(6)
14	R	3	14	F2	4	13	F1	1	1378.15588(2)	0.0322(2)	0.05(8)	-0.0083(1)	0.000058(3)
14	R	3	14	F2	6	13	F1	2	1443.85736(6)*	0.0488(3)	0.88(5)	-0.0092(3)	0.000018(11)
14	Q	3	14	A1	2	14	A2	1	1279.67272(3)	0.0350(2)	0.35(2)	-0.0046(1)	0.000062(3)
14	Q	3	14	F1	4	14	F2	1	1279.66774(7)	0.0264(4)			
14	Q	3	14	F1	5	14	F2	2	1290.63592(2)	0.0405(1)		-0.0036(1)	
14	Q	3	14	F1	10	14	F2	1	1365.85508(7)*	0.0500(8)	1.06(15)		
14	Q	3	14	F2	5	14	F1	1	1290.74068(2)	0.0446(1)	0.65	-0.0032(1)	
14	P	3	13	A1	3	14	A2	1	1223.97296(1)	0.0355(1)	0.92(2)	-0.0048(1)	0.000028(2)
14	P	3	13	A2	4	14	A1	1	1211.87736(1)	0.0432(0)	0.89(1)	-0.0037(0)	0.000019(1)
14	P	3	13	E	5	14	E	3	1201.64092(1)	0.0265(0)	0.75(1)	-0.0042(0)	0.000021(1)
14	P	3	13	E	6	14	E	2	1210.07726(1)	0.0413(1)	0.88(1)	-0.0043(0)	0.000025(1)
14	P	3	13	F1	7	14	F2	4	1201.13208(1)	0.0521(0)	1.06(1)	-0.0025(0)	0.000004(1)
14	P	3	13	F1	8	14	F2	3	1207.83322(1)	0.0520(0)	1.02(1)	-0.0033(0)	0.000022(1)
14	P	3	13	F1	9	14	F2	2	1216.62981(1)	0.0407(0)	0.89(1)	-0.0030(0)	0.000027(1)
14	P	3	14	F1	11	15	F2	1	1217.98304(2)	0.0307(1)	0.88(3)	-0.0036(1)	0.000010(4)
14	P	3	13	F1	10	14	F2	1	1223.99463(1)	0.0273(1)	0.05(3)	-0.0044(1)	-0.000073(4)
14	P	3	13	F2	8	14	F1	3	1202.42108(1)	0.0511(0)	1.07(1)	-0.0033(0)	0.000025(1)
14	P	3	13	F2	9	14	F1	2	1210.78397(1)	0.0505(0)	0.98(1)	-0.0042(0)	0.000027(1)
14	P	3	13	F2	10	14	F1	1	1216.32898(1)	0.0459(1)	0.98(1)	-0.0025(0)	0.000026(2)
15	R	3	15	A1	2	14	A2	1	1443.67612(4)*	0.0390(1)	0.90(4)	-0.0065(2)	0.000042(6)
15	R	3	15	A2	1	14	A1	1	1378.82657(1)	0.0400(0)	0.86(1)	-0.0037(0)	0.000026(1)
15	R	3	15	E	2	14	E	2	1378.50822(1)	0.0395(1)	0.90(1)	-0.0040(1)	0.000032(2)
15	R	3	15	E	4	14	E	1	1443.77905(9)*	0.0401(4)	1.12(10)	-0.0070(4)	-0.000022(16)
15	R	3	15	F1	1	14	F2	4	1377.00730(1)	0.0506(1)	1.05(1)	-0.0019(1)	0.000006(2)
15	R	3	15	F1	2	14	F2	3	1377.93562(1)	0.0498(1)	0.99(1)	-0.0010(0)	0.000005(2)
15	R	3	15	F1	3	14	F2	2	1380.26494(1)	0.0395(1)	0.90(1)	-0.0048(0)	0.000041(2)
15	R	3	15	F1	6	14	F2	1	1443.74437(6)*	0.0384(3)	1.03(7)	-0.0062(3)	-0.000032(11)
15	R	3	15	F2	1	14	F1	3	1377.24665(1)	0.0495(1)	1.11(1)	-0.0017(1)	0.000023(2)
15	R	3	15	F2	2	14	F1	2	1378.63177(1)	0.0485(1)	0.96(1)	-0.0041(0)	0.000029(2)
15	R	3	15	F2	3	14	F1	1	1380.20769(1)	0.0446(1)	0.88(1)	-0.0031(1)	0.000029(2)
15	Q	3	15	A1	2	15	A2	1	1287.63784(3)	0.0367(1)		-0.0041(1)	
15	Q	3	15	F2	4	15	F1	1	1275.94654(3)	0.0231(1)	0.89(3)	-0.0039(1)	0.000030(3)
15	Q	3	15	E	4	15	E	1	1287.72300(5)	0.0424(7)		-0.0018(6)	
15	Q	3	15	F1	6	15	F2	2	1287.69425(4)	0.0407(4)		-0.0030(3)	
15	P	3	14	A1	3	15	A2	2	1190.97320(1)	0.0518(1)	0.95(1)	-0.0025(1)	0.000012(1)
15	P	3	14	A1	4	15	A2	1	1210.00613(1)	0.0352(0)	0.74(1)	-0.0033(0)	0.000018(1)
15	P	3	14	A2	3	15	A1	1	1192.82798(1)	0.0501(1)	0.93(1)	-0.0039(0)	0.000031(1)
15	P	3	14	E	6	15	E	2	1199.69199(1)	0.0429(1)	0.98(1)	-0.0037(1)	0.000019(2)
15	P	3	14	E	7	15	E	1	1209.69452(1)	0.0416(1)	0.96(1)	-0.0022(1)	0.000016(2)
15	P	3	14	F1	8	15	F2	4	1191.47705(1)	0.0512(1)	1.00(1)	-0.0042(1)	
15	P	3	14	F1	9	15	F2	3	1202.72385(1)	0.0515(1)	1.06(1)	-0.0042(0)	0.000019(2)
15	P	3	14	F1	10	15	F2	2	1209.80531(1)	0.0414(1)	0.92(1)	-0.0030(0)	0.000016(1)
15	P	3	14	F2	8	15	F1	4	1192.06946(1)	0.0514(1)	1.00(1)	-0.0037(1)	0.00003(2)
15	P	3	14	F2	9	15	F1	3	1198.99851(1)	0.0527(1)	1.04(1)	-0.0025(0)	0.000021(2)
15	P	3	14	F2	10	15	F1	2	1204.03298(1)	0.0434(0)	0.95(1)	-0.0038(0)	0.000016(1)
15	P	3	14	F2	11	15	F1	1	1217.99560(2)	0.0290(1)	0.83(3)	-0.0050(1)	0.000045(3)
16	R	3	16	A1	1	15	A2	2	1381.15798(1)	0.0499(1)	1.05(1)	-0.0018(1)	
16	R	3	16	A1	2	15	A2	1	1384.96581(1)	0.0343(1)	0.82(2)	-0.0049(1)	0.000022(2)
16	R	3	16	A1	3	15	A2	1	1460.06905(10)*	0.0544(5)	1.51(10)	-0.0105(5)	0.000107(24)
16	R	3	16	A2	1	15	A1	1	1381.49377(1)	0.0464(1)	1.10(1)	-0.0022(1)	0.000033(2)
16	R	3	16	E	1	15	E	2	1382.30048(2)	0.0402(1)	0.92(2)	-0.0028(1)	0.000021(2)
16	R	3	16	E	2	15	E	1	1384.91296(3)	0.0420(2)	0.78(4)	-0.0022(2)	0.000042(7)
16	R	3	16	E	4	15	E	1	1459.47957(13)*	0.0365(8)			
16	R	3	16	F1	1	15	F2	4	1381.23551(2)	0.0502(1)	1.01(2)	-0.0030(1)	-0.000007(3)
16	R	3	16	F1	2	15	F2	3	1383.05216(2)	0.0503(2)	1.32(4)	-0.0012(2)	0.000014(8)
16	R	3	16	F1	3	15	F2	2	1384.93133(2)	0.0420(2)	0.77(4)	-0.0053(2)	-0.000005(6)
16	R	3	16	F1	4	15	F2	1	1387.98719(3)	0.0286(1)	1.02(2)	-0.0042(0)	0.000030(2)
16	R	3	16	F1	6	15	F2	2	1459.65716(13)*	0.0463(6)			
16	R	3	16	F2	1	15	F1	4	1381.33457(2)	0.0492(1)	1.10(1)	-0.0022(1)	0.000051(2)
16	R	3	16	F2	2	15	F1	3	1382.18277(2)	0.0498(1)	1.02(1)	-0.0049(1)	0.000028(2)
16	R	3	16	F2	3	15	F1	2	1383.24573(2)	0.0422(1)	0.86(1)	-0.0041(1)	0.000027(2)
16	R	3	16	F2	4	15	F1	1	1387.98933(6)	0.0286(1)	1.02(2)	-0.0042(0)	0.000030(2)
16	Q	3	16	F1	5	16	F2	1	1284.47514(4)	0.0366(1)		-0.0036(2)	
16	Q	3	16	F2	6	16	F1	2	1284.50323(4)	0.0396(2)		-0.0028(2)	

16	P	3	15	A1	4	16	A2	1	1194.95651(1)	0.0503(1)	1.10(1)	-0.0038(1)	0.000018(2)
16	P	3	15	A2	3	16	A1	2	1188.95368(1)	0.0528(1)	0.92(1)	-0.0033(1)	0.000014(2)
16	P	3	15	A2	4	16	A1	1	1211.97429(5)	0.0357(4)	1.11(6)	0.0003(2)	
16	P	3	15	E	6	16	E	3	1181.52849(1)	0.0184(0)	0.71(2)	-0.0047(0)	0.000031(1)
16	P	3	15	E	7	16	E	2	1196.50297(2)	0.0388(1)	0.95(2)	-0.0061(1)	0.000022(3)
16	P	3	15	E	8	16	E	1	1211.96704(5)	0.0193(3)			
16	P	3	15	F1	9	16	F2	4	1180.97148(1)	0.0505(1)	1.07(1)	-0.0027(1)	0.000018(3)
16	P	3	15	F1	10	16	F2	3	1191.43005(2)	0.0514(1)	0.82(2)	-0.0022(1)	0.000006(4)
16	P	3	15	F1	11	16	F2	2	1196.12048(2)	0.0464(1)	0.97(1)	-0.0027(1)	0.00002(3)
16	P	3	15	F1	12	16	F2	1	1203.18116(2)	0.0361(1)	0.86(1)	-0.003(1)	0.000011(2)
16	P	3	15	F2	8	16	F1	4	1182.10474(1)	0.0497(1)	1.06(1)	-0.0039(1)	0.000034(3)
16	P	3	15	F2	9	16	F1	3	1190.23664(2)	0.0532(1)	0.87(1)	-0.0036(1)	0.000020(3)
16	P	3	15	F2	10	16	F1	2	1203.03992(2)	0.0405(1)	0.95(1)	-0.0043(1)	0.000017(2)
17	R	3	17	A2	1	16	A1	2	1386.17333(2)	0.0495(1)	0.98(2)	-0.0013(1)	0.000007(3)
17	R	3	17	E	1	16	E	3	1385.44060(2)	0.0190(1)	0.59(3)	-0.0024(1)	0.000020(2)
17	R	3	17	E	2	16	E	2	1387.72409(3)	0.0388(1)	0.76(4)	-0.0041(1)	0.000019(5)
17	R	3	17	F1	1	16	F2	4	1385.34958(3)	0.0500(1)	1.06(2)	-0.0032(2)	-0.000007(4)
17	R	3	17	F1	2	16	F2	3	1386.64263(3)	0.0501(1)	0.86(2)	-0.0058(1)	0.000035(4)
17	R	3	17	F1	3	16	F2	2	1387.66842(3)	0.0460(2)	0.80(3)	-0.0061(2)	-0.000010(6)
17	R	3	17	F1	4	16	F2	1	1389.61530(2)	0.0334(2)	1.05(3)		
17	R	3	17	F2	1	16	F1	4	1385.53375(3)	0.0489(1)	1.07(2)	0.0001(2)	0.000022(4)
17	R	3	17	F2	3	16	F1	2	1389.59400(3)	0.0371(1)	0.86(3)	-0.0064(1)	
17	P	3	16	A1	4	17	A2	1	1184.46922(2)	0.0428(1)	0.88(2)	-0.0045(1)	0.000029(5)
17	P	3	16	A2	4	17	A1	1	1196.31783(2)	0.0399(1)	0.91(2)	-0.0035(1)	0.000017(3)
17	P	3	16	E	6	17	E	3	1170.90030(2)	0.0177(1)	0.74(4)	-0.0045(1)	0.000013(3)
17	P	3	16	E	7	17	E	2	1181.77640(3)	0.0356(2)	0.83(5)	-0.0051(2)	0.000022(7)
17	P	3	16	E	8	17	E	1	1196.44882(4)	0.0346(2)	0.91(5)	0.0015(2)	
17	P	3	16	F1	9	17	F2	4	1171.50789(2)	0.0480(1)	1.10(3)	-0.0033(2)	-0.000012(7)
17	P	3	16	F1	10	17	F2	3	1182.74345(2)	0.0514(1)	0.86(3)	-0.0043(1)	0.000015(6)
17	P	3	16	F1	11	17	F2	2	1188.39522(3)	0.0477(1)	0.81(3)	-0.0029(1)	0.000024(5)
17	P	3	16	F1	12	17	F2	1	1205.92670(2)	0.0275(0)	0.78(1)	-0.0037(0)	0.000028(1)
17	P	3	16	F2	9	17	F1	5	1170.43091(2)	0.0491(1)	1.15(3)	-0.0038(2)	-0.000002(7)
17	P	3	16	F2	10	17	F1	4	1179.82315(2)	0.0522(1)	1.00(3)	-0.0023(1)	0.000034(6)
17	P	3	16	F2	11	17	F1	3	1189.00004(3)	0.0423(2)	0.77(3)	-0.0037(2)	-0.000006(6)
17	P	3	16	F2	12	17	F1	2	1196.40641(3)	0.0371(1)	0.83(3)	-0.0036(1)	0.00001(5)
17	P	3	16	F2	13	17	F1	1	1205.93045(3)	0.0275(0)	0.78(1)	-0.0037(0)	0.000028(1)
18	R	3	18	A1	1	17	A2	1	1391.11546(3)	0.0402(1)	0.87(3)	-0.0030(1)	0.000022(5)
18	R	3	18	E	1	17	E	3	1389.54369(5)	0.0211(2)	0.78(7)	-0.0027(1)	0.000002(6)
18	R	3	18	E	2	17	E	2	1390.78663(6)	0.0364(3)	0.88(7)	-0.0042(3)	0.000031(10)
18	R	3	18	F1	1	17	F2	4	1389.65489(3)	0.0416(3)	1.25(6)		
18	R	3	18	F1	2	17	F2	3	1390.90801(5)	0.0496(3)	1.00(5)	-0.0033(3)	0.000023(10)
18	R	3	18	F1	3	17	F2	2	1392.12258(3)	0.0465(1)	1.00(3)	-0.0041(1)	0.000021(6)
18	R	3	18	F2	1	17	F1	5	1389.48096(5)	0.0455(2)			-0.000071(10)
18	R	3	18	F2	2	17	F1	4	1390.36205(5)	0.0494(3)	1.08(5)	-0.0008(3)	0.000008(10)
18	R	3	18	F2	3	17	F1	3	1392.19737(3)	0.0411(1)	0.99(3)	-0.0058(1)	0.000007(5)
18	P	3	17	A1	3	18	A2	2	1160.88151(5)	0.0488(2)	1.40(5)	-0.0037(2)	0.000090(10)
18	P	3	17	A2	4	18	A1	2	1159.34992(6)	0.0517(2)	1.43(5)	-0.0035(3)	-0.000054(11)
18	P	3	17	A2	5	18	A1	1	1181.74953(3)	0.0355(2)	0.70(5)	-0.0038(2)	0.000010(8)
18	P	3	17	E	7	18	E	3	1170.98754(7)	0.0386(3)	0.87(12)	-0.0066(3)	0.000022(17)
18	P	3	17	E	8	18	E	2	1181.08650(7)	0.0427(3)	0.87(10)	-0.0038(3)	0.000032(18)
18	P	3	17	E	9	18	E	1	1199.87443(6)	0.0177(2)	0.67(11)	-0.0017(2)	
18	P	3	17	F1	9	18	F2	5	1160.30238(8)	0.0502(3)	1.13(8)	-0.0037(4)	0.000104(17)
18	P	3	17	F1	10	18	F2	4	1170.19489(5)	0.0530(3)	1.34(9)	-0.0013(3)	-0.000140(19)
18	P	3	17	F1	11	18	F2	3	1175.80712(5)	0.0434(3)	0.79(7)	-0.0033(2)	0.000044(13)
18	P	3	17	F1	12	18	F2	2	1189.71356(5)	0.0338(2)	0.56(7)	-0.0037(2)	0.000012(9)
18	P	3	17	F2	10	18	F1	4	1159.80025(7)	0.0504(3)	1.00(8)	-0.0030(4)	-0.000039(16)
18	P	3	17	F2	11	18	F1	3	1173.64698(5)	0.0494(3)	1.31(8)	-0.0033(3)	0.000061(17)
18	P	3	17	F2	12	18	F1	2	1181.33166(5)	0.0424(2)	0.87(7)	-0.0023(2)	0.000038(13)
18	P	3	17	F2	13	18	F1	1	1189.66338(5)	0.0366(2)	0.60(7)	-0.0033(2)	0.000005(10)
19	R	3	19	A1	1	18	A2	2	1393.80746(4)	0.0459(2)	1.23(5)	-0.0028(3)	0.000010(8)
19	R	3	19	A2	1	18	A1	2	1393.55446(4)	0.0495(2)	1.36(5)	-0.0026(3)	-0.000015(10)
19	R	3	19	A2	2	18	A1	1	1396.68695(5)	0.0354(4)	0.96(9)	-0.0041(4)	0.000047(14)
19	R	3	19	F1	1	18	F2	5	1393.68706(7)	0.0475(4)	1.44(8)	-0.0023(6)	0.000042(13)
19	R	3	19	F1	3	18	F2	3	1395.36504(7)	0.0453(7)	0.59(14)	-0.0016(8)	0.000120(24)
19	R	3	19	F2	1	18	F1	4	1393.61303(7)	0.0494(4)	0.94(8)	-0.0008(6)	-0.000004(13)
19	R	3	19	F2	2	18	F1	3	1395.15396(7)	0.0503(8)	1.29(14)	-0.0033(9)	0.000092(30)
19	R	3	19	F2	3	18	F1	2	1396.64174(9)	0.0411(8)	1.29(16)	-0.0038(9)	0.000048(32)
19	P	3	18	A1	4	19	A2	2	1159.54114(12)	0.0532(5)	0.60(13)	-0.0026(5)	0.000035(28)
19	P	3	18	A1	5	19	A2	1	1182.98600(6)	0.0301(2)	1.00(11)	-0.0039(3)	0.000030(15)
19	P	3	18	A2	4	19	A1	1	1164.98443(11)	0.0539(3)		-0.0041(4)	
19	P	3	18	E	8	19	E	2	1167.54534(10)	0.0368(5)			
19	P	3	18	E	9	19	E	1	1182.94420(15)	0.0313(8)	0.44(32)		
19	P	3	18	F1	12	19	F2	3	1173.79506(11)	0.0404(5)	0.89(21)	-0.0041(5)	-0.000028(33)
19	P	3	18	F1	13	19	F2	2	1182.95865(12)	0.0330(6)	1.60(23)		
19	P	3	18	F2	12	19	F1	3	1166.99444(8)	0.0471(5)			

19	P	3	18	F2	13	19	F1	2	1174.11090(10)	0.0362(4)	0.56(20)	-0.0035(5)	0.000104(28)
20	R	3	20	F1	2	19	F2	4	1398.63823(22)	0.0559(24)	0.33(40)	0.0039(24)	-0.000048(86)
20	R	3	20	F1	5	19	F2	1	1407.27456(7)	0.0129(2)	0.91(15)	-0.0055(2)	0.000047(8)
20	P	3	19	A1	5	20	A2	1	1166.39921(13)	0.0386(7)			

[a] Positions are given in cm^{-1}.

[b] Air-broadened half width and air-shift coefficients are in units of $cm^{-1}atm^{-1}$ at 296 K.

[c] Temperature depencence exponents of air-broadened half width coefficients are unitless.

[d] Temperature dependences of air-shift coefficients are in units of cm^{-1} atm^{-1} K^{-1}.

Uncertainties of measured parameters are given in parentheses in units of the last digit quoted.

* Forbidden transitions.

Figure(s)

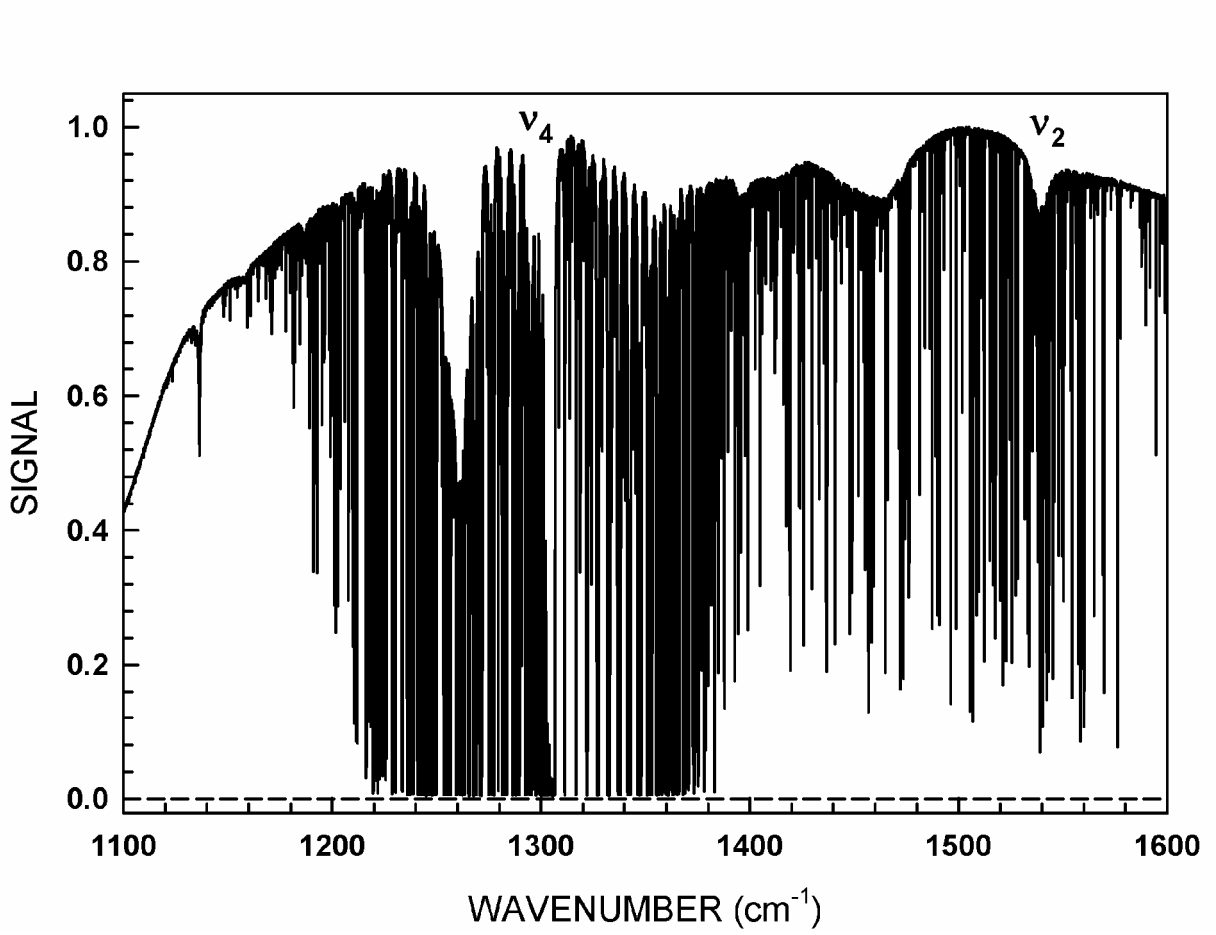

Figure 1

Figure(s)

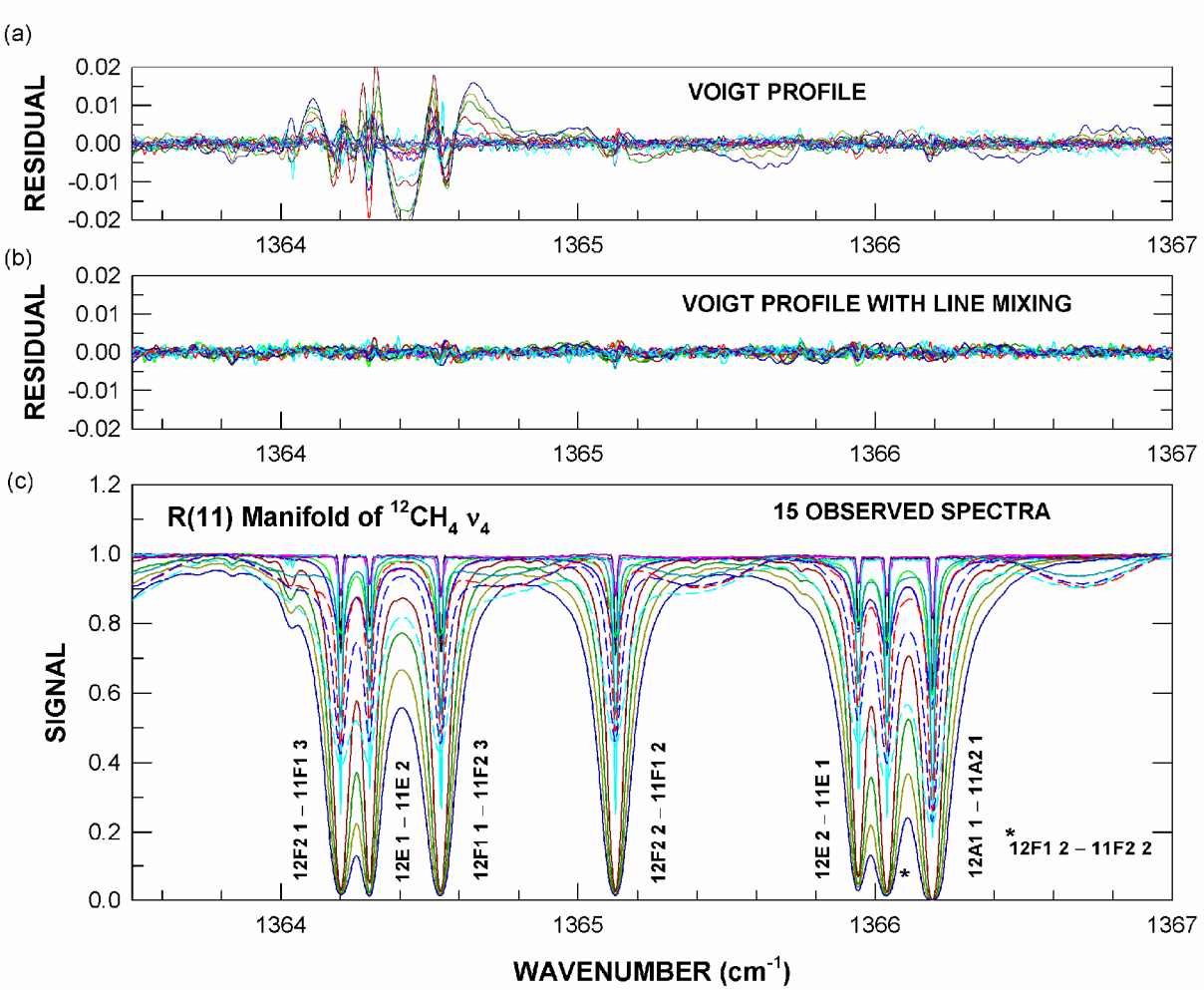

Figure 2

Figure(s)

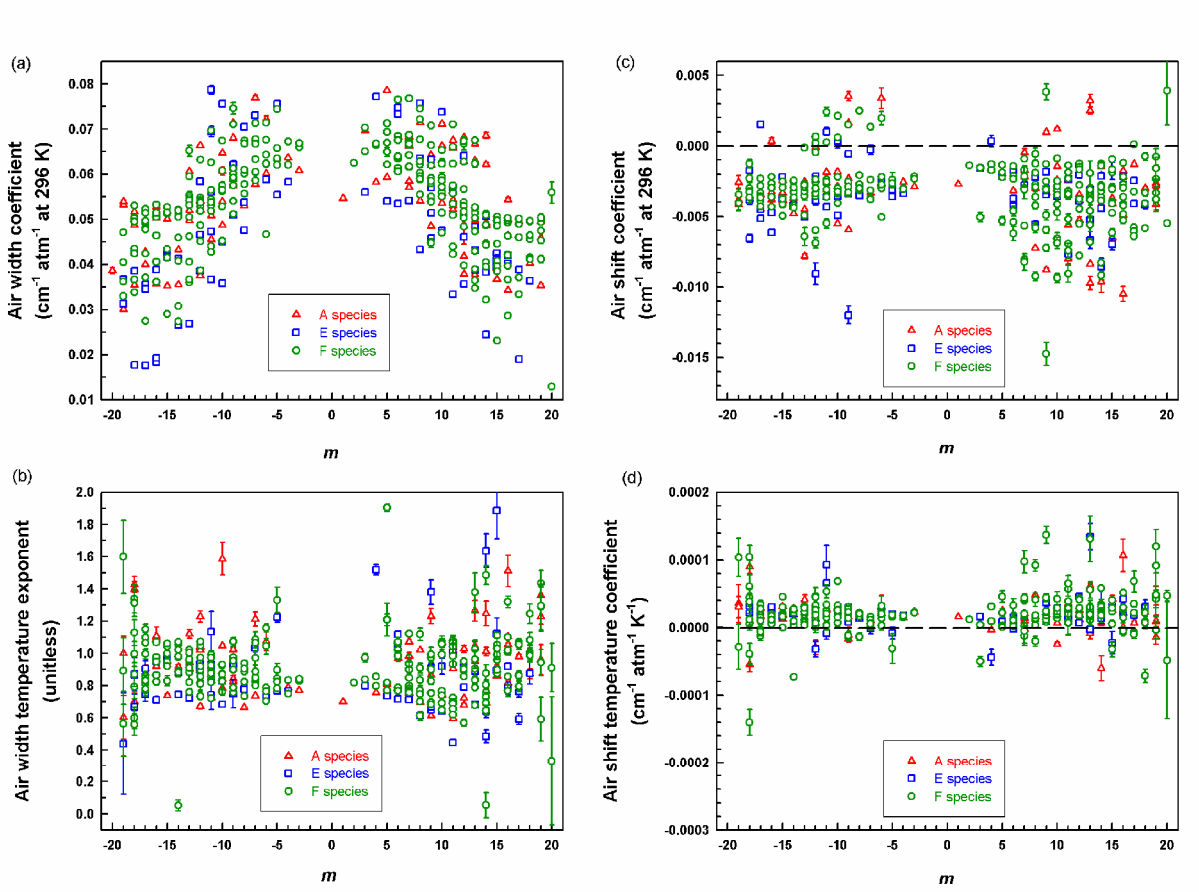

Figure 3

Figure(s)

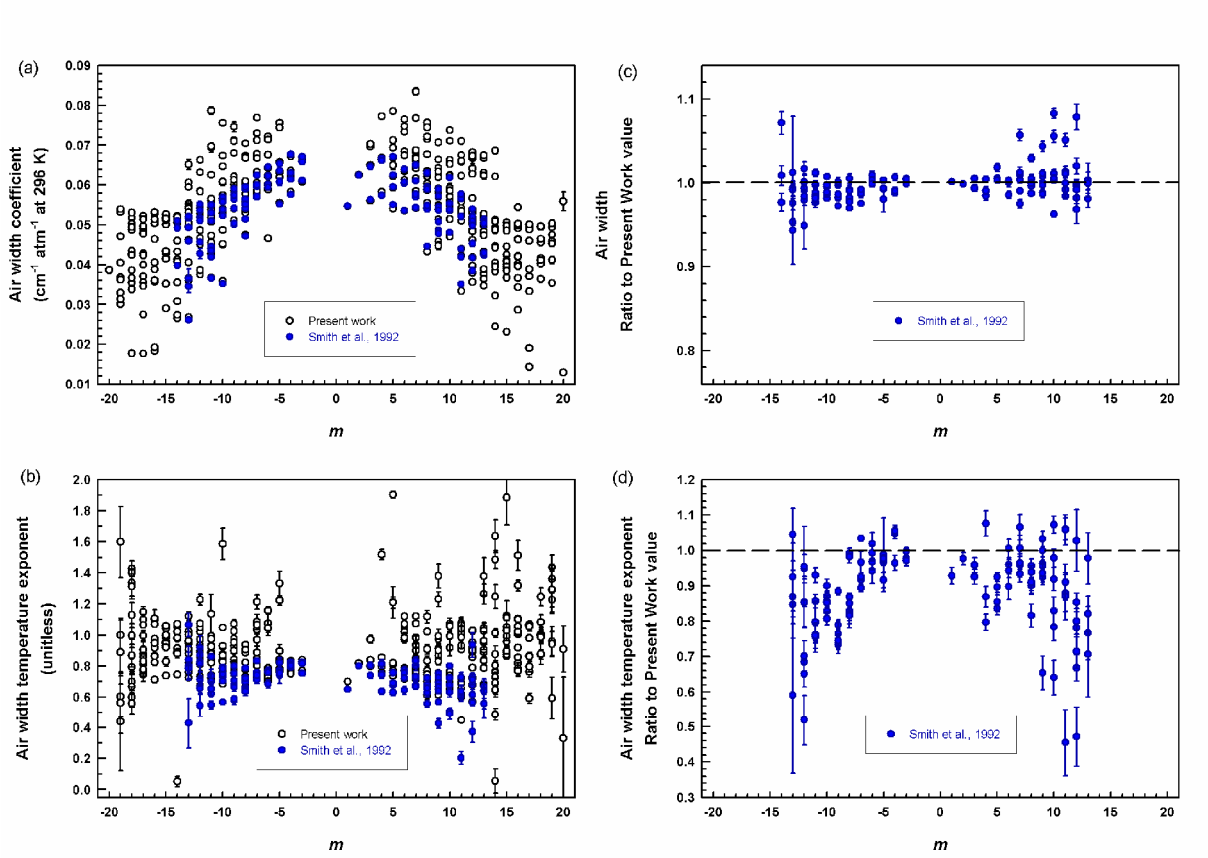

Figure 4

Figure(s)

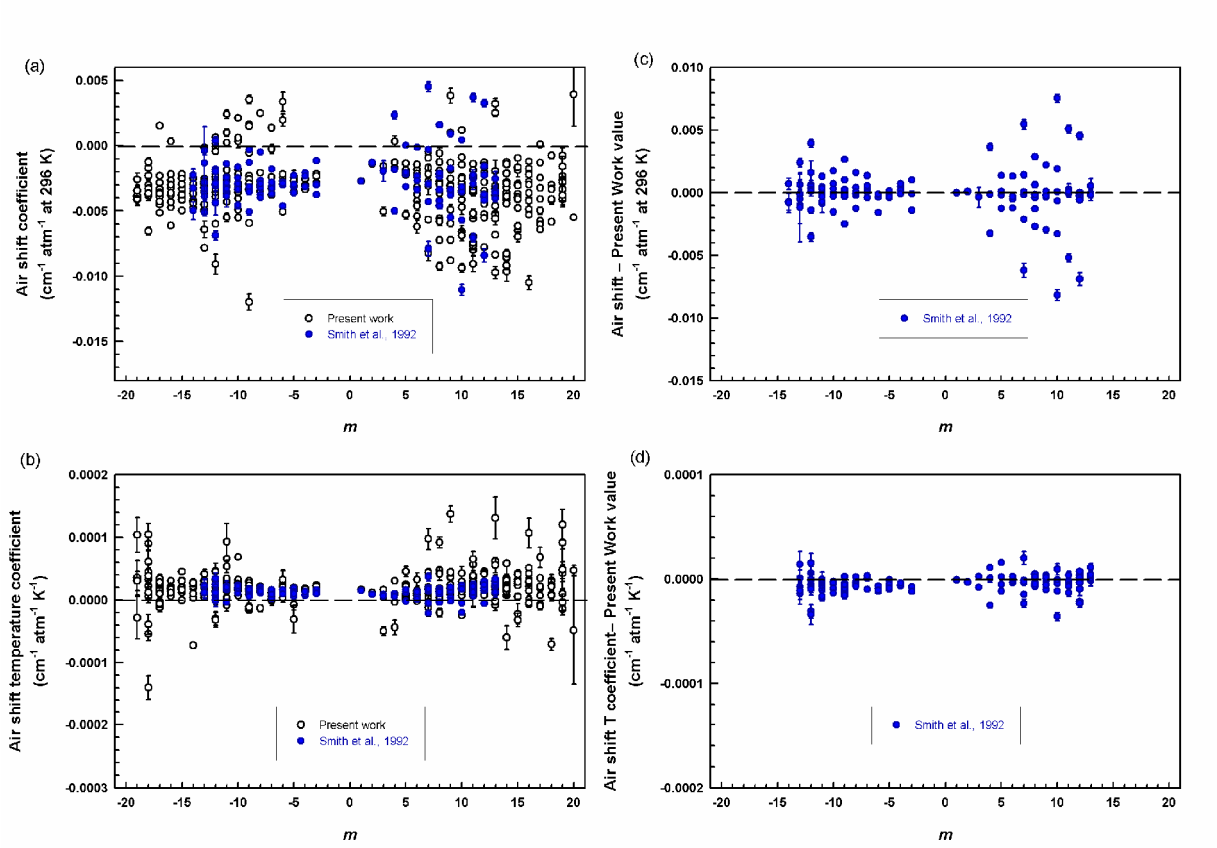

Figure 5

Figure(s)

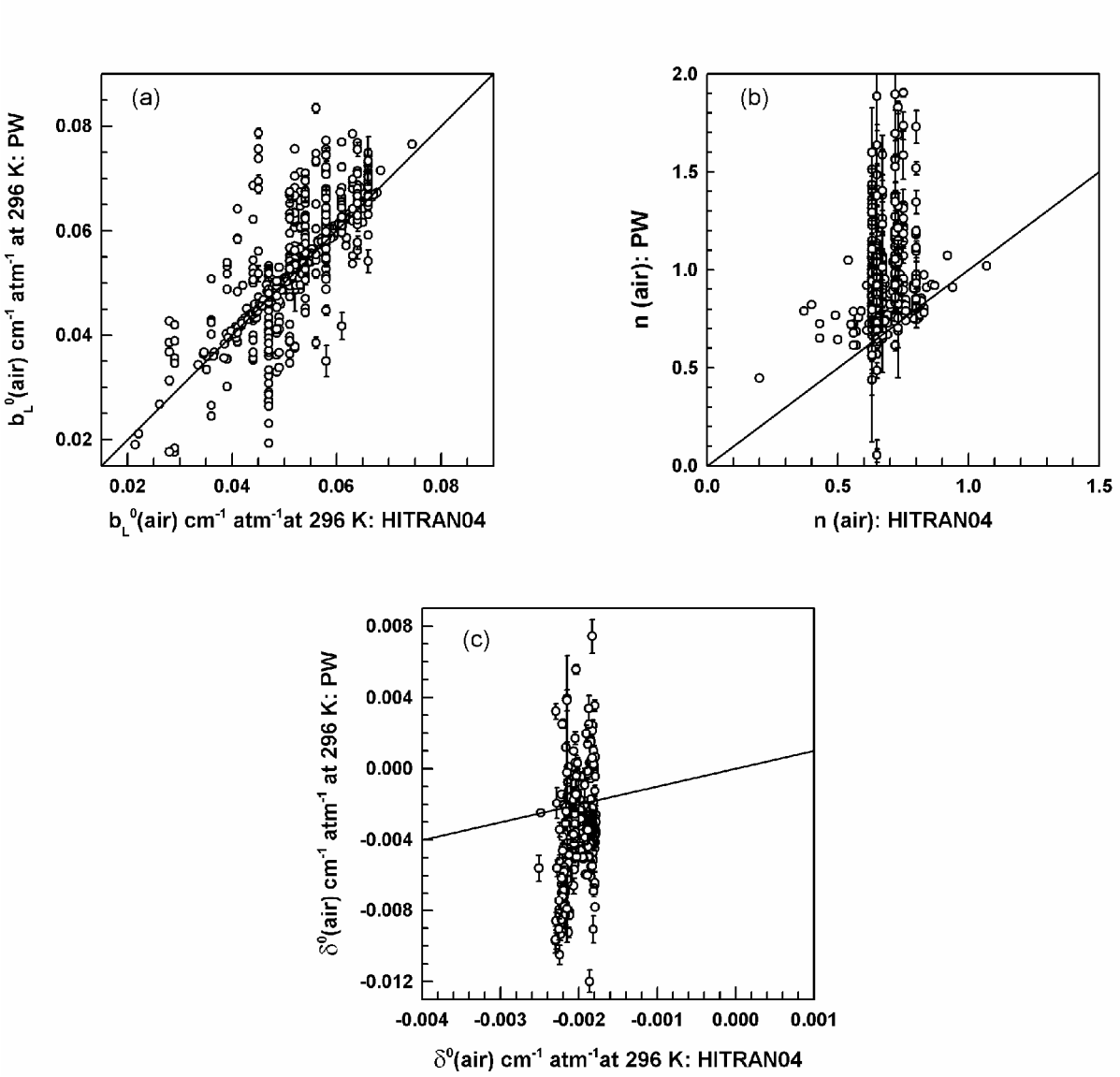

Figure 6

Figure(s)

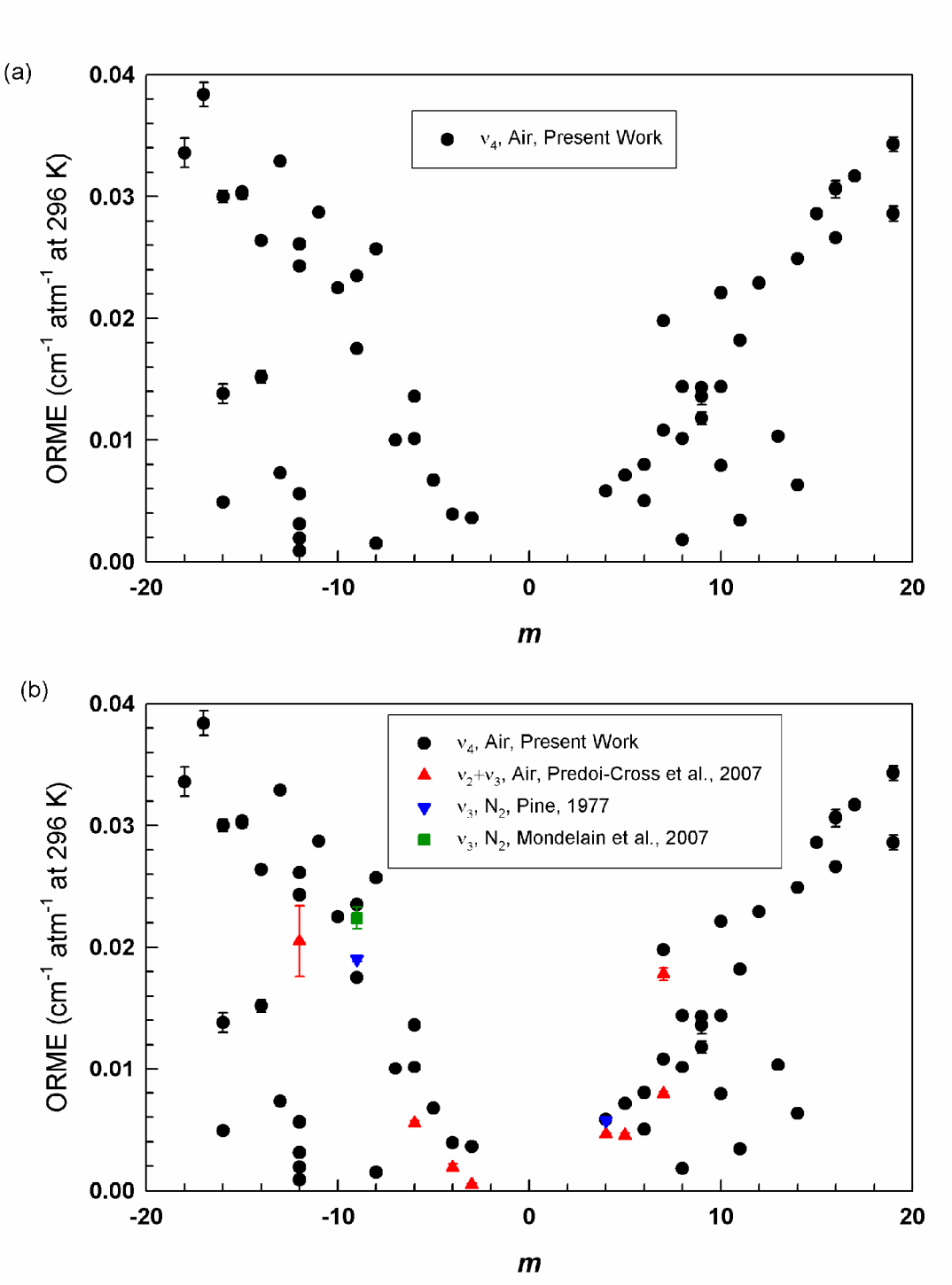

Figure 7